Lineage-specific intersection of endothelin and GDNF signaling in enteric nervous system development

Denise M. Poltavski[1*], Alexander T. Cunha[1*], Jaime Tan[1], Henry M. Sucov[2], and Takako Makita[1]

1 Darby Children's Research Institute, Department of Pediatrics, Medical University of South Carolina, Charleston, SC 29425, USA

2 Department of Regenerative Medicine and Cell Biology, Medical University of South Carolina, Charleston, SC 29425, USA

* These authors contribute equally to this work

Corresponding author: Takako Makita (makita@musc.edu)

Abstract

Two major ligand-receptor signaling axes – endothelin Edn3 and its receptor Ednrb, and glial-derived neurotrophic factor (GDNF) and its receptor Ret – are required for migration of enteric nervous system (ENS) progenitors to the hindgut. Mutations in either component cause colonic aganglionosis, also called Hirschsprung disease. Here, we have used Wnt1Cre and Pax2Cre in mice to show that these driver lines label distinct ENS sublineages during progenitor migration and in their terminal hindgut fates. Both Cre lines result in Hirschsprung disease when combined with conditional *Ednrb* or conditional *Ret* alleles. In vitro explant assays and analysis of lineage-labeled mutant embryos show that GDNF but not Edn3 is a migration cue for cells of both lineages. Instead, Edn3-Ednrb function is required in both for GDNF responsiveness, by expanding the Ret^+ population in the Pax2Cre lineage and by supporting Ret function in Wnt1Cre-derived cells. Our results demonstrate that two sublineages of progenitors give rise to the ENS, and that these divergently utilize endothelin signaling to support migration to the hindgut.

Introduction

The enteric nervous system (ENS) is the largest division of the peripheral nervous system and harbors a complex circuitry. Approximately a half billion enteric neurons in human (and over a million in mice) distribute along the entire axis of the gastrointestinal tract to regulate a variety of physiological functions (Furness, 2006). Colonic peristalsis that promotes defecation is controlled by several subtypes of enteric neurons that reside in the myenteric plexus that is located between the longitudinal and circular muscles of the gut. Colonic myenteric mechanosensory neurons are multiaxonal (Dogiel type II) neurons of which one axonal branch extends to the gut mucosa and synapses with mechanosensory (enterochromaffin) cells, while the opposite branches synapse on motor neurons or interneurons in neighboring myenteric ganglia. When mucosal enterochromaffin cells are stimulated by the presence of feces, mechanosensory endings are activated and then transmit signals through interneurons to activate or inhibit motor neurons, which generate contraction or relaxation of colonic circular muscle, resulting in peristalsis. This neural circuitry enables the ENS to sustain autonomous gut motility in the absence of central nervous system input.

The entirety of the ENS is thought to arise exclusively from migratory neural crest cells. This conclusion was based primarily on avian intraspecies cell transplantation (Le Douarin, 1982) and dye labelling studies (Serbedzija, Bronner-Fraser, & Fraser, 1989), and subsequently supported by genetic labelling studies of the neural crest cell lineage in mice (Kapur, 2000; Yamauchi et al., 1999). Enteric neural crest cells originate from two distinct sources. Most arise from the vagal region of the hindbrain and cervical spinal cord, migrate first to the foregut, and then continue to migrate along and colonize the entire length of the gut. Once in the gut, these organize into intrinsic ganglia, including the colonic myenteric plexus that has primary control of gut motility. A distinct sacral neural crest cell population colonizes the hindgut, migrating from the distal end of hindgut in a

cranial direction (Anderson RB, 2000). The majority of sacral neural crest cells constitute the pelvic ganglia that are located on the rectal wall and project rostrally along the colon to supply sympathetic and parasympathetic control of gut physiology, but not including colonic peristalsis (Keast, 1995). Neural crest clearly contributes substantially to the ENS, and while past studies could not formally exclude a contribution from other sources, there has also been no experimental observation that would invoke the involvement of any other developmental origin.

Defective caudal migration of enteric progenitors results in aganglionosis in the terminal bowel. This has no consequence in fetal life while gut motility is suppressed, but after birth, when fecal progression through the hindgut requires a functional ENS circuitry, absence of adequate ENS function leads to congenital gut motility disorders, characterized by the inability to defecate and involuntary fecal retention. In such cases, the hindgut expands to accommodate the accumulating material, accounting for one name of this condition as congenital megacolon. A synonymous term for this pathology is Hirschsprung disease.

Hirschsprung disease is an inherited or sporadic condition in humans, and is associated with mutations in genes encoding two pairs of extracellular ligand/receptor signaling molecules: the endothelin ligand EDN3 and its G-protein coupled receptor EDNRB, and the receptor tyrosine kinase RET and its ligand GDNF (Parisi & Kapur, 2000). Mice that carry mutations in these genes lack an enteric plexus in the distal colon and therefore phenocopy the human condition (Baynash et al., 1994; Durbec, Larsson-Blomberg, Schuchardt, Costantini, & Pachnis, 1996; Hosoda et al., 1994; Sanchez et al., 1996; Schuchardt, D'Agati, Larsson-Blomberg, Costantini, & Pachnis, 1994). Hirschsprung disease can present alone or as a component of Waardenburg-Shah syndrome that includes deafness and pigmentation abnormalities, reflecting the contributing role of these signaling pathways in other tissues, but colonic aganglionosis is the defining condition of this disease. Hirschsprung disease is also a prototypical example of a large class of congenital syndromes and adult cancers collectively called

neurocristopathies that involve neural crest cells as a common etiologic factor (Mueller & Goldstein, 2022).

Placodes are bilateral condensations of the surface ectoderm that generate migratory neurons and other cell types in a manner that is similar to neural crest (Baker & Bronner-Fraser, 2001). Placodes and neural crest jointly contribute to many cranial ganglia, including the Xth cranial (vagus/nodose) ganglia. While neural crest gives rise to a variety of neuronal subtypes and glia, neurogenic placodes are only known to give rise to sensory neurons (D'Amico-Martel & Noden, 1983). The contribution of the placode cell lineage has only been recognized in the head but never before associated with the ENS.

In the accompanying paper (Tan, Duron, Sucov, & Makita, 2023), we used Pax2Cre to label the placode lineage and Wnt1Cre to label the neural crest cell lineage in mice to demonstrate their contributions to specific components of the auditory system. As documented in past studies (Barald & Kelley, 2004; D'Amico-Martel & Noden, 1983; Ladher, O'Neill, & Begbie, 2010) and as reiterated in the accompanying paper with Pax2Cre and Wnt1Cre as lineage markers (Tan et al., 2023), the placode and neural crest cell lineages have distinct and independent fates in the inner ear. Auditory functionality requires endothelin (specifically Edn3) signaling through the endothelin receptor Ednrb in both lineages, although these requirements are separable and ñ□ñ□ñ□ñ□ñ□ñ□ñ□ñ□ñ□In this study, we have used Pax2Cre and Wnt1Cre to address the contribution of these

In this study, we have used Pax2Cre and Wnt1Cre to address the contribution of these cell lineages to the ENS. We demonstrate that CGRP-immunoreactive colonic myenteric mechanosensory neurons are uniquely labeled by Pax2Cre, whereas NOS^+ inhibitory motor neurons are uniquely derived from the Wnt1Cre lineage. Importantly, Edn3-Ednrb, a signaling axis previously defined to be important for enteric neural crest cell migration, also controls the migration of Pax2Cre-labeled enteric progenitor cells, such that conditional *Ednrb* mutation driven by Pax2Cre or Wnt1Cre both result in compromised gut motility. We further show that GDNF-

Ret signaling is required in both lineages to support ENS progenitor cell migration, albeit in a manner that intersects with Edn3-Ednrb signaling differently in Wnt1Cre-derived and Pax2Cre-derived cells. Our findings implicate a dual lineage origin for the ENS with mechanistically distinct features, and illuminate the consequences of Edn3 and GDNF signaling that account for Hirschsprung disease when either is compromised.

Results

Impaired colonic peristalsis in the absence of Pax2Cre-derived ENS cells in the distal colon

In the accompanying study addressing the placode lineage contribution to auditory development in mouse models for Waardenburg-Shah syndrome, we generated neural crest-specific (using Wnt1Cre) and placode-specific (using Pax2Cre) conditional *Ednrb* homozygous mutant mice (designated as *Wnt1Cre/Ednrb* and *Pax2Cre/Ednrb* respectively). In the outbred ICR background of our colony, we found that neither *Wnt1Cre/Ednrb* mutant nor *Pax2Cre/Ednrb* mutant mice lived beyond 3 weeks of age (Tan et al., 2023). The postnatal lethality of *Wnt1Cre/Ednrb* mutants around day P21 was predicted because of the well-established role of Edn3-Ednrb signaling in enteric neural crest migration and colonization (Baynash et al., 1994; Hosoda et al., 1994). However, the occurrence (and full penetrance) of lethality around this same time in *Pax2Cre/Ednrb* mutants was unexpected, as there was no prior implication that placode cells contribute to the ENS or do so in an endothelin signaling-dependent manner. *Pax2Cre/Ednrb* mutant mice exhibited growth retardation and reduced weight gain comparable to global *Ednrb* and conditional *Wnt1Cre/Ednrb* mutants in the second postnatal week (Figure 1a, 1b). Dissection and inspection of the gastrointestinal tract revealed that *Pax2Cre/Ednrb* mutants suffer from colonic distention and constriction similar to global *Ednrb* and *Wnt1Cre/Ednrb* mutant mice (Figure 1d), associated with near complete abrogation of defecation (Figure 1c). These observations indicate that *Ednrb*-deficiency in the Pax2Cre lineage impaired colonic peristalsis.

To visualize the contribution of Pax2Cre-derived cells to the ENS and its dependence on endothelin signaling, we crossed the *R26*^{lacZ} reporter into the *Pax2Cre/Ednrb* background and visualized Pax2Cre-labled cells during ENS progenitor cell migration and colonization. We conducted a parallel analysis for the Wnt1Cre lineage. Fate mapping with *Pax2Cre/R26*^{lacZ} in normal embryos showed labeled cells reaching the midgut loop at E11.5, reaching the mid-hindgut junction at E12.5, and nearly completing the colonization of the hindgut by E13.5 (Figure 1 – figure supplement 1f-h, Figure 1e). A comparable pattern was observed with Wnt1Cre-derived migratory cells (Figure 1 – figure supplement 1b-d, Figure 1g), and this temporal pattern has been previously observed using a variety of non-lineage-dependent markers of enteric progenitors (Lake & Heuckeroth, 2013). *Ednrb*-deficient Pax2Cre lineage labeled cells (Figure 1f) and *Ednrb*-deficient Wnt1Cre-derived cells (Figure 1h) both failed to advance beyond the cecum by E12.5, and this ultimately resulted in a lack of cells from both lineages in the distal colon (hindgut-derived) of postnatal mice (Figure 1j, 1m). *Pax2Cre/R26*^{lacZ} and *Wnt1Cre/R26*^{lacZ} mice homozygous for a global *Edn3* mutant allele also exhibited an absence of lineage-labeled cells in the distal colon (Figure 1k, 1n), demonstrating that migration failure is for lack of endothelin signaling and not some artifact of the conditional *Ednrb* allele. *Edn3* ligand was expressed normally in the developing guts of both *Ednrb* conditional mutant backgrounds (Figure 1f, 1h). These results indicate that the Wnt1Cre lineage and the Pax2Cre lineage both populate the hindgut, and that both lineages utilize Edn3-Ednrb signaling for migration and colonization of the hindgut.

<u>Wnt1Cre and Pax2Cre define distinct ENS cell lineages</u>

In the inner ear, the distinct and nonoverlapping fates of the Pax2Cre and Wnt1Cre cell lineages correspond precisely to placodal and neural crest fates as defined by prior studies (Tan et al., 2023). In addition to all known placode progeny (e.g. otic vesicle (Figure 1 – figure supplement 1i) and its later derivatives in the inner ear and cranial ganglia (Figure 1 – figure supplement 1j-l), Pax2Cre is active in several other cell types. Pax2Cre activity

was detected in the ventral half of the neural tube (Figure 1 – figure supplement 1i), which does not overlap the Wnt1Cre-active (dorsal) domain. Additional Pax2Cre active cell types include limb mesenchyme (Figure 1 – figure supplement 1e) and intermediate mesoderm and its derivatives (the mesonephric ducts and then later also in the ureteric bud) (Figure 1 – figure supplement 1e, 1o), although these sources are not migratory or neurogenic. Pax2Cre activity was not detected in several known postotic cranial/cardiac and trunk neural crest derivatives including dorsal root ganglia and sympathetic ganglia (Figure 1 – figure supplement 1m, 1n) and mesenchyme of the cardiac outflow tract (Figure 2 – figure supplement 1c). Despite this specificity, a trivial explanation for the occurrence of Hirschsprung disease phenotypes in both *Wnt1Cre/Ednrb* and *Pax2Cre/Ednrb* mutants could be if both Cre drivers recombine in the same cell populations of the ENS. As it is not possible to combine the two Cre alleles together to visualize their separate (or potentially overlapping) recombination domains, we addressed this by using molecular markers at the initial onset of their embryonic migration and in terms of the terminal (postnatal) fates of each lineage.

First, we examined the expression domain of Pax2 protein with respect to the recombination domains of Pax2Cre and Wnt1Cre at the very early enteric progenitor migratory stage (E9.5-10.0). Pax2 staining was prominent in the lens and otic vesicle (both known placode derivatives), in intermediate mesoderm (future kidneys), and germane to this report also in the postotic pharyngeal arches that abut vagal neural crest (Figure 2 – figure supplement 1a-b). Pax2 protein overlapped Pax2Cre-labeled pharyngeal ectoderm and Pax2Cre-labeled mesenchymal cells just at the stage of delamination from the ectoderm, although Pax2 expression was downregulated with migration and therefore not detected in most Pax2Cre lineage-labeled mesenchymal cells in the postotic domain (Figure 2 – figure supplement 1c-d). In contrast, Pax2 expression was excluded from the territory of pharyngeal neural crest marked by the Wnt1Cre lineage label (Figure 2 – figure supplement 1e-f).

We also examined expression of neural crest markers AP2 (Mitchell, Timmons, Hebert, Rigby, & Tjian, 1991) and Sox10 (Southard-Smith, Kos, & Pavan, 1998). AP2 and Sox10 were both detected within postotic migratory pharyngeal cells (Figure 2 – figure supplement 2a-b). We observed that the entirety of Wnt1Cre-labeled cells expressed AP2 (Figure 2 – figure supplement 2e-f). Sox10 expression was associated with a subset of the Wnt1Cre-labeled cell population, and thus with a subset of AP2-expressing arch mesenchymal cells (Figure 2 – figure supplement 2e-f). In contrast, although there was overlap of AP2 expression with Pax2Cre in the ectoderm, neither AP2 nor Sox10 were expressed in any migratory Pax2Cre lineage-labeled cells (Figure 2 – figure supplement 2g-h).

Finally, we examined the enteric progenitor marker Ret during the early stage of enteric progenitor migration in the gut (E10.0-10.5) in *Pax2Cre/R26*$^{nT\text{-}nG}$ and *Wnt1Cre/R26*$^{nT\text{-}nG}$ embryos by 2-color immunohistochemistry for nuclear-GFP and Ret (Figure 2). We quantified the number of nGFP-positive, Ret-positive, and nGFP and Ret-double positive cells; cells that did not express either the lineage marker or Ret were excluded from measurement as these are indistinguishable from all other cell types that are present in the gut. In *Pax2Cre/R26*$^{nT\text{-}nG}$ embryos (4 embryos from different litters, total 288 counted cells), the vast majority of Pax2Cre-derived cells did not express Ret during this period (Figure 2a-c): 24% of the countable cells were Pax2Cre-derived, yet only 1.6% expressed Ret (Figure 2v). The remaining 76% of countable cells were Pax2Cre-negative and Ret-expressing (Figure 2v) and presumably originate from the Wnt1Cre lineage. We performed the same analysis for the Wnt1Cre lineage, finding that the majority of Wnt1Cre-derived cells expressed Ret (Figure 2g-i). Quantification (n=4; 185 cells) revealed that 72% of Wnt1Cre-derived cells expressed Ret and only 2.0% of cells expressed Ret but were Wnt1Cre lineage-negative (these are presumably Pax2Cre-derived, which was directly measured at 1.6% as described above) (Figure 2v). In both analyses, we cannot directly identify cells of the opposite lineage (i.e., nGFP-negative) that do not express Ret. However, we assume that the Ret-negative

nGFP-positive fraction (grey bars) of each lineage corresponds to the Ret-negative and nGFP-negative population in the other lineage, and this was approx. 20% of counted cells in both cases. These results indicate that the majority of Wnt1Cre-derived cells at E10.5 in the midgut express Ret whereas only a minor population of Pax2Cre-derived cells does so, and further support the idea that Pax2Cre and Wnt1Cre delineate molecularly distinct populations of migratory ENS progenitor cells.

As summarized earlier, colonic peristalsis is facilitated by an integrated circuitry from mechanosensory neuron to interneuron to motor neuron to muscle contraction (Figure 3a). Electrophysiology studies of guinea pig colon showed that mechanosensory neurons release the excitatory neurotransmitter calcitonin gene related peptide (CGRP) to initiate peristaltic contractions (Sarna, 2010). By immunostaining, we identified that $CGRP^+$ neurons in the postnatal P9 mouse distal colon are located in the myenteric plexus and send their projections through villi to the gut luminal epithelium, consistent with a mechanosensory fate (Figure 3b). In the human and guinea pig intestine, nitric oxide synthase (NOS) is recognized as a marker for both inhibitory interneurons and inhibitory motor neurons (Costa et al., 1992; Timmermans et al., 1994). We found in mouse that NOS^+ neurons are found in the myenteric ganglia and their axons are found exclusively within the circular muscle layer (Figure 3c), implying that these represent at least a subset of motor neurons. Interneurons are not readily identifiable with this circular cross section analysis because of their exclusively interganglionic (mostly ascending/descending) projections.

To discern the lineage origins of these mature cell types, we evaluated the expression of these markers in P9 pups that were also lineage labeled with Pax2Cre or Wnt1Cre crossed with *R26* reporters. First, based on morphology and expression of the pan-neuronal marker Hu, approximately half of colonic myenteric ganglion cells were labeled with either lineage marker (Figure 3 – figure supplement 1a-b, 1g pie chart). If these Cre lines are completely non-overlapping in their recombination domains, this implies that all or almost all neurons are

derived from either a Pax2Cre or a Wnt1Cre lineage. In contrast, only approximately one-third of neurons were CGRP$^+$ or NOS$^+$ (Figure 3 – figure supplement 1g white bars, 1h pie chart), which means that additional neuronal fates are taken by both lineages (which is expected). Strikingly, the vast majority (>90%) of CGRP$^+$ neurons of the distal colon were Pax2Cre-derived (Figure 3d, Figure 3 – figure supplement 1c-d, 1h bar graph). A minimum number of CGRP$^+$ neurons were labeled by Wnt1Cre (Figure 3f, Figure 3 – figure supplement 1, 1h bar graph), and these may not even be vagal neural crest-derived, since some sacral neural crest-derived pelvic ganglion axons and their associated cell bodies also express CGRP (Figure 3 – figure supplement 2) but are not colonic mechanosensory neurons (Keast, 1995). These results indicate that Wnt1Cre-derived cells have little or no commitment to a mechanosensory fate in the distal colon. The majority of NOS$^+$ neurons were derived from the Wnt1Cre lineage (Figure 3g, Figure 3 – figure supplement 1f, 1h bar graph), although Pax2Cre-derived neurons also gave rise to a NOS-reactive population of the distal colon (Figure 3e, Figure 3 – figure supplement 1e, 1h bar graph). As mentioned above, NOS identifies both inhibitory interneurons and inhibitory motor neurons in the intestine, so these results do not by themselves indicate if Pax2Cre-labeled NOS$^+$ and Wnt1Cre-labeled NOS$^+$ neurons are the same or different fates (this point is addressed below in lineage-specific *Ednrb* mutants).

If Pax2Cre and Wnt1Cre label distinct subsets of ENS neurons in normal mice, a prediction is that these subsets might be selectively ablated in lineage-specific *Ednrb* mutant mice. To address this, we immunohistochemically analyzed axonal projections from the myenteric plexus in serial sections of the colons of both lines of mutant mice at P9. Importantly, sections were taken at the transition area where lineage-labeled cells are present (Figure 3 – figure supplement 3c, 3g), rather than from the more distal colon where no cells are present to stain (Figure 3 – figure supplement 3d, 3h). Adjacent sections were stained for CGRP or NOS. We observed a profound reduction of CGRP$^+$ axons projecting towards the enteric lumen in *Pax2Cre/Ednrb* mutant guts (Figure 3j, 3p), equal to that in global *Ednrb* mutants (Figure 3i, 3p), whereas NOS$^+$ axons in the circular muscle were present normally in the adjacent section (Figure 3n, 3q). There were some CGRP$^+$ axons projecting longitudinally along

the submucosal layer (Figure 3j asterisks), although these most likely originate from pelvic ganglia as described above (Figure 3 – figure supplement 2) and were also detected in the global *Ednrb* mutant gut (Figure 3i asterisks). *Wnt1Cre/Ednrb* mutant guts exhibited abundant CGRP$^+$ axons projecting toward sensory epithelium (Figure3k, 3p) while their circular muscle layers showed a total loss of NOS$^+$ axonal innervation (Figure 3o, 3q). NOS$^+$ neurons were still present in the myenteric plexus of the *Wnt1Cre/Ednrb* mutant distal colon (Figure 3o inset arrowhead); as these neurons project neither to sensory nor motor targets, we suspect that these are interneurons and likely originate from the Pax2Cre lineage. Thus, in the transition area, defective migration of Pax2Cre-derived enteric progenitor cells results in selective loss of myenteric mechanosensory neurons, while myenteric motor neurons and their innervations of the circular muscle were not affected. Reciprocally, defective migration of Wnt1Cre-derived ENS progenitors results in selective loss of motor neurons with no impact on the mechanosensory neuron population.

These results collectively suggest that Pax2Cre-labeled and Wnt1Cre-labeled cells have a distinct and nonoverlapping marker expression program during their embryonic migration, and have a distinct set of terminal differentiation fates in the postnatal gut. A further conclusion from the analysis of conditional *Ednrb* mutants is that neither lineage can modulate its normal fate to compensate for the absence of the other.

Pax2Cre lineage-specific *Ret* mutant embryos exhibits defective enteric progenitor migration

ENS development requires a functional GDNF-Ret signaling axis alongside that of Edn3-Ednrb. The unexpected observation that Ednrb function is required in both the Wnt1Cre and Pax2Cre domains in ENS development led us to also address Ret function in these lineages. A previous study (Luo et al., 2007) documented Hirschsprung disease phenotypes in mice with conditional Ret mutation in the Wnt1Cre domain (*Wnt1Cre/Ret* mutants), including lethality around postnatal day 21. Global *Ret* deficiency results in neonatal lethality because of renal agenesis (Durbec et al., 1996; Schuchardt et al., 1994), and because Pax2Cre is expressed in intermediate

mesoderm, *Pax2Cre/Ret* mutants also die in the early postnatal period for the same reason (data not shown). We therefore explored the consequences of *Ret* deficiency in the Pax2Cre lineage during embryonic enteric progenitor cell migration. In *Pax2Cre/Ret/R26*^{lacZ} mutant embryos at E12.5, we observed an obvious deficiency of Pax2Cre-labeled cells migrating throughout the midgut, and no Pax2Cre-labeled cells migrated caudally beyond the cecum (Figure 4b), whereas lineage-labeled cells reached the terminal hindgut in littermate controls (Figure 4a). This result implies a function for Ret within the Pax2Cre lineage, which was surprising because the expression analysis described above indicated that Ret is only expressed in a small percent of the Pax2Cre lineage at the earlier E10.5 timepoint (Figure 2a-c, 2v).

We considered whether Ret expression in the Pax2Cre lineage changes around E10.5 that might account for these observations. We found that a substantially larger fraction of Pax2Cre-labeled cells in the distal midgut (at the migratory wavefront) in control E11.5 *Pax2Cre/R26*$^{nT\text{-}nG}$ embryos expressed Ret (Figure 2m, 2y black bar) relative to E10.5 (Figure 2w, black bar). This demonstrates that the Pax2Cre-labeled population in control embryos expands significantly during the E10.5-11.5 period. This could occur by proliferation of the very small Ret^{+} population that was present at E10.5, or could occur by conversion of Ret^{-} to Ret^{+} cells within the lineage, or both, and perhaps was already just underway at E10.5. Obviously, at both E10.5 and E11.5, there were no Ret^{+} cells in the Pax2Cre lineage in *Pax2Cre/Ret* mutants (Figure 2n-o, 2w, 2y).

We next performed wholemount staining with the neural progenitor marker p75 (at E10.5) or with the pan-neuronal marker 2H3 (at E12.5) on guts isolated from *Pax2Cre/Ret/R26*$^{td\text{-}Tomato}$ mutants and their littermate controls. This allowed us to visualize the Pax2Cre lineage in *Pax2Cre/Ret* mutant embryos alongside other neuronal lineages (i.e., the Wnt1Cre lineage) in which Ret function is intact. At E10.5, p75-expressing enteric progenitors included Pax2Cre lineage cells co-migrating with non-Pax2Cre cells (Figure 4i), the latter which presumably consists of Wnt1Cre-derived cells. In *Pax2Cre/Ret* mutant embryos at this stage, p75-expressing cells

again included those with and without the Pax2Cre lineage label, demonstrating a normal caudal progression (Figure 4j). Histological Ret expression analysis in *Pax2Cre/Ret/R26*$^{nT\text{-}nG}$ embryos clearly showed that some migratory progenitor cells express Ret (Figure 2d-f). Since *Ret* is knocked out in *Pax2Cre/Ret* mutants, these Ret^{+} cells are presumed to be Wnt1Cre-derived. Quantitative evaluation, however, indicated that overall ENS progenitor cell number was already affected as early as E10.5 in the *Pax2Cre/Ret* mutant background (Figure 2w): both the Pax2Cre-derived cell population and the Ret-expressing non-Pax2Cre population were reduced by half, and therefore the total number of countable cells (expressing one or both markers) per midgut from each mutant embryo was also reduced by half. A somewhat larger reduction in total countable cells was observed in *Pax2Cre/Ret* mutants at E11.5 (Figure 2y) compared to E10.5 (Figure 2w). Consequently, at E12.5, compared to control littermate (Figure 4e), *Pax2Cre/Ret* mutants showed a marked deficiency of 2H3-positive cells though the midgut loop, and no 2H3 signal was detected caudal to the cecum (Figure 4f). The interpretation of this analysis is that *Ret* deficiency in the Pax2Cre lineage impacts ENS progenitor cells derived from the Pax2Cre lineage as well as from the presumptive Wnt1Cre lineage, starting as the migratory cells enter the midgut.

In parallel we also crossed the conditional *Ret* allele into the *Wnt1Cre/R26* background. Wnt1Cre-labeled cells populated the esophagus and stomach but failed to migrate into the intestine (Figure 4d), which recapitulates the global *Ret* mutant phenotype (Durbec et al., 1996; Schuchardt et al., 1994). Wholemount 2H3 staining confirmed the total loss of enteric progenitor cells along the entire axis of the developing intestine (Figure 4h). Defective progenitor entry into the intestinal tract was evident as early as E10.5 based on wholemount p75 staining (Figure 4i) as well as Ret expression analysis on histological sections prepared from *Wnt1Cre/Ret/R26*$^{nT\text{-}nG}$ embryos at E10.5 (Figure 2j-l, 2x) and E11.5 (Figure 2q, 2z). These results demonstrate that Ret function in the Wnt1Cre domain is absolutely required for migration of all enteric progenitors, Wnt1Cre-derived as well as non-Wnt1Cre-derived (i.e., Pax2Cre-derived), into and through the intestinal tract.

Ret is required for Pax2Cre-derived ENS progenitor cells migration and colonization

To better understand how GDNF-Ret signaling influences the Pax2Cre and Wnt1Cre lineage cells, we employed collagen gel explant cultures of serial 200μm slices prepared from E10.5 midgut segments collected in a rostrocaudal sequence (Figure 5 – figure supplement 1a). After 3 days in culture we visualized td-Tomato as a lineage marker, stained for Hu as a neuronal marker, and BLBP as a glial marker. No outgrowth was observed in the absence of added factors (Figure 5a). Hu and BLBP were both detected in the untreated explanted gut slices (Figure 5a), showing that enteric progenitor cells present in the gut slices survived for three days in vitro and sustained a normal differentiation program without growth factors. GDNF induced robust radial outgrowth from control midgut slices, which included a mixed population of neurons and glia; Pax2Cre lineage cells were present in these outgrowths (Figure 5b). Control explants showed a progressively diminishing response along the rostrocaudal axis (Figure 5g), which reflects the number of enteric progenitor cells present in each slice. *Pax2Cre/Ret* mutant gut explants, however, exhibited little or no outgrowth in response to GDNF (Figure 5c, 5g), even though lineage-positive, Hu-positive, and BLBP-positive cells are present in the explant itself. Importantly, because Ret-expressing non-Pax2Cre lineage (likely Wnt1Cre-derived) cells are present throughout the midgut at E10.5 (Figure 2f, 2w), yet there were no lineage negative outgrowths in response to GDNF in *Pax2Cre/Ret* explants (Figure 5c), this indicates that the Wnt1Cre-derived cells do not harbor a cell-autonomous response to GDNF.

Control E10.5 *Wnt1Cre/R26*$^{td\text{-}Tomato}$ midgut explants demonstrated response to GDNF at each axial level (Figure 5d-e, h), similar to *Pax2Cre/R26*$^{td\text{-}Tomato}$ explants. *Wnt1Cre/Ret* mutant gut explants showed no lineage marker, neuronal Hu, or glial BLBP positive cells along the entirety of the midgut segments, within or outgrown from the explant (Figure 5f, 5h), confirming the total absence of all enteric progenitor cells in this mutant background (Figure 4d). Collectively, we interpret these results to show that ENS progenitor migration is an orchestrated process that requires GDNF response in both Pax2Cre and Wnt1Cre progenitor populations.

Ednrb-expressing enteric progenitor migration is not promoted by Edn3 but GDNF-Ret signaling

Edn3-Ednrb and GDNF-Ret signaling are both required for caudal migration of the Wnt1Cre-derived and Pax2Cre-derived enteric progenitors. We used the gut slice explant assay to address the relationship between these signaling mechanisms. Midgut slices from *Pax2Cre/R26*$^{td\text{-}Tomato}$ and *Wnt1Cre/R26*$^{td\text{-}Tomato}$ embryos were cultured in collagen beds supplemented with EDN3 or with the p75 ligand NGF for 3 days in vitro. While explanted gut sections at E10.5 contain cells that express p75 and Hu, neither EDN3 nor NGF promoted enteric progenitor cell outgrowth compared to the activity of GDNF (Figure 5 – figure supplement 2). Similarly, at E11.5, EDN3 and NGF induced only minimal outgrowth from both Pax2Cre- and Wnt1Cre-lineage labeled midgut sections (Figure 6 – figure supplement 1). Impaired cell migration in vivo (Figure 1f, 1h) has at various times been previously interpreted in global *Edn3* and *Ednrb* mutants to represent a chemoattractive role for Edn3-Ednrb signaling, but as previously shown in vitro (Barlow, de Graaff, & Pachnis, 2003; Goto et al., 2013; Nagy & Goldstein, 2017) and in our results, Edn3-Ednrb signaling does not by itself induce migration of either Pax2Cre-labeled or Wnt1Cre-labeled enteric progenitors.

Edn3-Ednrb signaling is an upstream regulator of Ret signaling in a lineage specific manner

The in vitro explant assays clearly demonstrate that GDNF-Ret signaling is the major mechanism that supports ENS progenitor migration. To address why enteric progenitor migration in vivo is defective in *Ednrb*-deficient backgrounds, we performed gut slice explant assays using E11.5 midguts isolated from *Pax2Cre/Ednrb/R26*$^{td\text{-}Tomato}$ and *Wnt1Cre/Ednrb/R26*$^{td\text{-}Tomato}$ mutant embryos. Across the rostral-caudal axis of the midgut, *Pax2Cre/Ednrb* mutant explants showed a blunted response to GDNF compared to control cells (Figure 6a, 6c), which was more severe at the distal end (Figure 6b, 6d, 6i-j), even though lineage-positive cells were present. *Wnt1Cre/Ednrb* mutant midgut segments exhibited a similar trend as *Pax2Cre/Ednrb* mutant midgut in both proximal (Figure 6e, 6g, 6k) and distal segments (Figure 6f, 6h, 6l), including greater impairment of GDNF

responsiveness at the migratory wavefront. These results show that the Pax2Cre and Wnt1Cre lineages both rely on endothelin signaling to fully populate the gut with GDNF-responsive cells, and imply that endothelin signaling is needed to support GDNF responsiveness in enteric progenitors. A similar interpretation for the aggregate ENS progenitor population was made previously using wild-type tissue treated with a combination of GDNF and Edn3 (Barlow et al., 2003).

Next we asked whether *Ednrb*-deficiency alters Ret expression in the enteric progenitor cell population. We used 2-color IHC for nuclear-GFP and Ret on histological sections prepared from E11.5 *Pax2Cre/Ednrb/R26*$^{nT\text{-}nG}$ mutant embryos and their littermate controls. As also noted earlier (Figure 2m, 2y), in normal E11.5 embryos a large fraction of Pax2Cre-derived cells express Ret at the migratory wavefront (Figure 7a, 7e). In the *Pax2Cre/Ednrb* mutant, however, Pax2Cre-labeled cells populating the apex of the midgut loop were Ret-negative, and the surrounding Ret-expressing cells were mostly unlabeled by the Pax2Cre lineage marker (Figure 7b, 7f). We measured the number of nGFP-positive only, Ret-positive only, and nGFP and Ret double positive cells at three different axial levels: distal midgut, caudal half of the proximal midgut (towards the cecum; equivalent to 0-600 microns in Figure 6i) and rostral half of the proximal midgut (towards the foregut-midgut junction; equivalent to 600-1200 microns in Figure 6i). The analysis confirmed that absence of *Ednrb* resulted in far fewer Pax2Cre lineage-derived cells expressing Ret in the more caudal segments (Figure 7i). Thus, the expansion of the Ret^{+} subpopulation of the Pax2Cre lineage that occurs between E10.5-11.5 (Figure 2m, 2y) requires Ednrb signaling in a cell autonomous manner. As noted earlier, this could occur via proliferation of the very small Ret^{+} population at E10.5, by induction of Ret expression in previously Ret-negative cells, or both. The important conclusion is that this process by Pax2Cre-derived cells is dependent on Ednrb.

We performed the same analysis for E11.5 *Wnt1Cre/Ednrb/R26*$^{nT\text{-}nG}$ mutants and their littermate embryos (Figure 7c-d, 7g-h, 7j). Unlike the observation in the Pax2Cre lineage, Edn3-Ednrb signaling does not affect Ret

expression in Wnt1Cre-derived migratory enteric progenitor cells. Nonetheless, these cells are unable to respond to GDNF in vivo (Figure 1h) and in vitro (Figure 6g-h).

In general, extracellular ligands of receptor tyrosine kinases (RTKs) trigger autophosphorylation of intracellular tyrosine residues that ultimately recruit intracellular adaptor proteins to initiate downstream signaling. In a variety of ways, RTK signaling can require mediation by G protein coupled receptors, a mechanisms called transactivation (Kilpatrick & Hill, 2021). Prior in vitro explant studies have implicated a convergence of Ret and Ednrb at the level of protein kinase A activity ((Barlow et al., 2003; Goto et al., 2013); see also Discussion), although other mechanisms of transactivation have been described for Ednrb to other RTKs (Grantcharova et al., 2006; Harun-Or-Rashid, Konjusha, Galindo-Romero, & Hallbook, 2016), and Ret with other GPCRs (Tsuchioka, Takebayashi, Hisaoka, Maeda, & Nakata, 2008). Because Ret expression was preserved in Wnt1Cre-derived enteric progenitors even as they were nonresponsive to GDNF, we considered that transactivation via Ednrb might be involved. To address this, we fluorescently visualized the phosphorylation status of Ret (i.e., its degree of activation) in Wnt1Cre-derived cells in the midgut loop of E11.5 *Wnt1Cre/Ednrb/R26*$^{nT\text{-}nG}$ mutants and their littermate embryos. Confocal z-stack images showed that Ret protein was detected in both the cytoplasm and nucleus of Wnt1Cre-labeled migratory cells (Figure 7k-n, cyan; nuclear localization of Ret and many other RTKs has been previously noted (Chen, Hsu, & Hung, 2020; Chen & Hung, 2015) and is not unusual). An antibody specific for phospho-Ret Y1015 was detected in the majority (87%) of control Wnt1Cre-labeled cells (Figure 7q), also in the cytoplasm and nucleus (Figure 7k, magenta). However, phospho-Y1015 signal was only evident in 33% of *Ednrb*-deficient Wnt1Cre-derived cells (Figure 7l, 7q). Thus, a substantial subpopulation of the Wnt1Cre lineage requires Ednrb for Ret Y1015 phosphorylation. Because Ednrb is expressed only in a subset of Wnt1Cre-derived enteric progenitor cells (Figure 7 – figure supplement 1), the residual Y1015 phosphorylation observed in *Wnt1Cre/Ednrb* mutant cells is likely to occur in the Ednrb-negative Wnt1Cre-derived cell population. Interestingly, *Ednrb*-deficiency did not affect phosphorylation of Ret-Y1096 as demonstrated by positive staining

in the Wnt1Cre^{+}; Ret^{+} nuclei (Figure 7n, 7r). Furthermore, phospho-Y1096 staining was also notable within the Wnt1Cre-unlabled cell population (nGFP-negative, presumptively of the Pax2Cre lineage), although in these cells, both Ret and phospho-Y1096 Ret showed cell surface rather than nuclear localization (Figure 7o-p), suggesting that Ret signaling may be deployed differently in the Pax2Cre lineage. Although we (or other studies) have not yet proven the biological importance of Ret Y1015 in enteric progenitor migration, our results demonstrate that at least one feature of active Ret signaling in Wnt1Cre lineage cells requires the presence of Ednrb.

Discussion

Using the Wnt1Cre and Pax2Cre lines, in this study we have deconstructed the involvement of the two major signaling axes (GDNF/Ret and Edn3/Ednrb) in enteric nervous system development. We have provided new insights on the mechanistic convergence between these signals and on the etiology of Hirschsprung disease.

The ENS has long been thought to derive solely from the neural crest. Our study reveals that the ENS has a dual lineage origin as defined by the Pax2Cre and Wnt1Cre drivers. It is important to clarify that we define these lineages by function (recombination profile) rather than by anatomy. It is tempting to assume that these correspond strictly to placode and neural crest, respectively, as they do in craniofacial development (cite accompanying paper). Nonetheless, for ENS progenitors this is not proven. Thus for example, it is formally possible that these recombination territories for ENS progenitors include different subdomains of neural crest rather than neural crest vs. placode, and if so this would still fit the definition of dual lineages. For this reason we were careful in this manuscript to describe the "Pax2Cre lineage" and the "Wnt1Cre lineage" rather than interpret these as placode and neural crest. Regardless, we present a compelling argument that these represent at least mostly distinct sublineages of the ENS: their gene expression profiles differ in early progenitor migration,

their utilization of GDNF/Ret and Edn3/Ednrb signaling is distinct, the E12.5 consequences of Ret-deficiency in the two lineages are radically distinct, and most importantly at least some of their terminal differentiation fates in the hindgut are unique. These latter two observations also preclude the possibility that Pax2Cre becomes active in migratory Wnt1Cre-derived cells. It is implausible that even a moderate percentage of the Pax2Cre lineage overlaps with the Wnt1Cre lineages, as there are too many Ret^{+} cells that are not labeled by either lineage marker individually (Figure 2v-z). In the end, the goal of this study was to elucidate mechanisms by which the Pax2Cre and Wnt1Cre lineages utilize GDNF and Edn3 signaling to populate the hindgut, rather than challenge the conclusion of a neural crest origin of the ENS. While our observations may prompt reevaluation of this longstanding conclusion, to address this question properly would require a range of approaches and reagents that are beyond the scope of the present study.

We observed that cells of the Pax2Cre and Wnt1Cre lineages co-mingle in the pharyngeal region and co-migrate through the gut. Indeed our observations indicate that gut migration by each lineage is dependent on the other. We cannot yet explain this behavior. Neural crest cells are known to migrate as an interconnected network, a property called collective cell migration (Theveneau & Mayor, 2012), and it is possible that Pax2Cre-derived cells incorporate into the same. The 20% of cells of both lineages that do not express Ret (Figure 2v, grey bars) may also use this mechanism to support their migration. Within this assembly, the different roles of each lineage are unknown. Possible explanations for their required co-dependence could include unique abilities of each to attach to or degrade different components of the matrix, or some sort of paracrine activity that maintains collective migration. The net effect in normal development would be to bring both sets of progenitor cells to the same points of the gut at the same time, which might facilitate terminal assembly of circuitry. This observation of codependent migration might explain in part why the role of the Pax2Cre lineage was never previously recognized: were a subcomponent of the ENS able to migrate normally in neural crest ablation studies, the phenotypic result would likely not be described as aganglionosis.

Defecation is a function that is selectively accomplished by the myenteric plexus of the distal colon, where the integrated circuitry of mechanosensory nerves, excitatory and inhibitory interneurons, and excitatory and inhibitory motor nerves causes what are called “giant migrating contractions” that push fecal material forward (Sarna, 2010). This is a unique neurophysiological process of the distal colon and is distinct from the spontaneous rhythmic contractions that occur with the passage of chyme (partially digested food) along the earlier axis of the gastrointestinal tract. In postnatal mice of each conditional *Ednrb* mutant background, in the proximal colon where cells of both lineages successfully migrate, we observed a selective loss of CGRP mechanosensory neurons in the *Pax2Cre/Ednrb* background, and a selective loss of NOS^+ inhibitory motor neurons in the *Wnt1Cre/Ednrb* background. This observation is informative for demonstrating the developmental potential of each lineage, and corresponds to the fate of each lineage in normal mice, but is representative of only a very specific domain of the mutant guts. The explanation for Hirschsprung disease in both conditional *Ednrb* mutants is the deficiency of both lineages in the distal colon, combined with the selective loss of specific neuronal subtypes in more cranial domains.

Using *Ret* conditional knockout, we observed that the Wnt1Cre and Pax2Cre lineages differ significantly in their use of GDNF signaling. Thus, the Wnt1Cre lineage required GDNF responsiveness to migrate into the foregut, whereas the Pax2Cre lineage migrated into the midgut and only became GDNF-dependent at the hindgut. This behavior corresponds to expression of Ret in the early stages of Wnt1Cre-derived cells, and later abundance of Ret expression in Pax2Cre-derived cells. Alternative factors present in the foregut may uniquely support migration of the Pax2Cre lineage, but other explanations are possible.

Our studies demonstrate that Edn3 signaling through Ednrb is required to support GDNF responsiveness and thereby to support cell migration in both the Pax2Cre and Wnt1Cre lineages. We describe independent

mechanisms to explain this relationship: Ret expression is induced or expanded by Ednrb signaling in Pax2Cre-derived cells, whereas in Wnt1Cre-derived cells, Ednrb induces competence for Ret signaling without changing Ret expression. It should be clear that we have not yet proven that either role is functionally required for normal ENS development, so for the present these are still candidate mechanisms.

Past studies have made a strong argument that protein kinase A (PKA) is a downstream point of convergence between endothelin signaling and Ret activity in enteric progenitor cell migration (Barlow et al., 2003; Goto et al., 2013). Because many if not all cell types express PKA, whereas Ret is specific for ENS progenitors, we instead asked if the activity of Ret (as indicated by its level of phosphorylation) is influenced by endothelin signaling in the Wnt1Cre lineage. Interestingly, we determined that phosphorylation of Ret Y1015 requires Ednrb activity in Wnt1Cre-derived cells. Phosphorylation of this residue is known to activate the PLCg/PKC pathway. For practical reasons, in this study we only investigated phospho-Y1015 and phosphor-Y1096, and other modification sites or types might be more relevant to explain the relation between Ednrb and Ret in enteric progenitors of the Wnt1Cre lineage. In any event, the conceptual conclusion that Edn3-Ednrb signaling converges on GDNF-Ret function in both the Pax2Cre and Wnt1Cre lineages is supported by both the in vitro and in vivo observations and helps to explain the common phenotype of Hirschsprung disease that is seen when any component is mutated.

Our analyses have delineated the dual lineage origins of $CGRP^+$ mechanosensory and NOS^+ inhibitory motor neurons of the distal colonic circuitry, but clearly there is vastly more complexity in the ENS that is yet to be understood. Myenteric ganglia contain additional neural and glial subtypes that are still uncharacterized for lineage origin and function. Furthermore, the small intestine and proximal colon have their own physiology and functions, and it is expected that the ENS sustains the autonomy of these components of the gut through additional specialized circuits that respond to appropriate stimuli and execute different commands from those in

the distal colon. As Wnt1Cre-derived and Pax2Cre-derived cells both colonize the foregut and midgut as well as the hindgut, we speculate that each lineage may also be allocated to distinct fates and functions in order to complete a functional circuitry in these parts of the gut.

We were able to define the distinct contributions of the Wnt1Cre and Pax2Cre lineages to the ENS using appropriate genetic strategies in mice. Cell-based transplantation approaches to restore bowel function in Hirschsprung disease infants are currently focused only on neural crest cells, for example as derived by directed differentiation from pluripotent stem cells. To fully reconstitute a functional ENS circuitry in patients, it will be necessary to ensure that these transplanted cells have the capacity to differentiate into the full range of ENS cell types, including mechanosensory neurons.

With the same null mutation of *Ednrb*, the severity of Hirschsprung disease is highly dependent on strain background in rats (Dang et al., 2011) and mice (Hosoda et al., 1994). This indicates the existence of unlinked alleles that modify the consequences of *Ednrb*-deficiency. Similarly, in humans, Hirschsprung disease-associated mutations are almost always heterozygous (presumably haploinsufficient), but show variable extent of phenotypic penetrance, even so far as to be inherited in some affected patients from one asymptomatic parent (Fuchs et al., 2001). In some cases, the genetic background effect involves a mutation in a gene already known to be associated with Hirschsprung disease: a human genome-wide association study demonstrated genetic interaction between the *EDNRB* and *RET* loci (Carrasquillo et al., 2002), and synergy was evident in mice with intentional combinations of *Ednrb* and *Ret* (McCallion, Stames, Conlon, & Chakravarti, 2003) or *Ednrb* and *Sox10* (Cantrell et al., 2004) alleles. Clearly there is opportunity to discover new genes that do not independently cause Hirschsprung disease but which modify the penetrance of the known set of genes. In this light, it was striking that mice on an ICR background with conditional or global *Ednrb* deficiency die uniformly at 3 weeks of age. ICR mice are an outbred background with a genetic mixture of many poorly characterized ancestral sources

(Aldinger, Sokoloff, Rosenberg, Palmer, & Millen, 2009) and have been maintained as an internally crossed (but not inbred) breeding colony by many providers. Interestingly, in congenital sensorineural deafness, the other major EDN3-EDNRB phenotype that with Hirschsprung disease defines Waardenburg-Shah syndrome type IV, the penetrance of hearing impairment in ICR-background Edn3 or *Ednrb* mutant mice is variable (approx. 50%)(Tan et al., 2023). This indicates that different modifiers interact with Edn3-Ednrb in auditory development vs. enteric nervous system development. These mouse models may help to clarify the additional components and downstream pathways that result in human Hirschsprung and Waardenburg-Shah pathologies.

Materials and Methods

Animals. Ednrb (Rattner, Yu, Williams, Smallwood, & Nathans, 2013) (JAX:011080), *Edn3* (Baynash et al., 1994) (JAX:002516), *Ret* (Luo et al., 2007) (JAX:028548), *Pax2Cre* (Ohyama & Groves, 2004), *Wnt1Cre* (Danielian, Muccino, Rowitch, Michael, & McMahon, 1998), *ROSA26*^{lacZ} (Soriano, 1999), *ROSA26*$^{CAG\text{-}tdTomato}$ (Madisen et al., 2010) (JAX: 007914), *ROSA26*$^{nT\text{-}nG}$ (Prigge et al., 2013) (JAX: 023537), *ROSA26*^{EYFP} (Srinivas et al., 2001) (JAX:006148), *Ednrb-EGFP* (Gong et al., 2007) (MMRRC_010620-UCD) alleles have been described previously. Wild-type ICR mice used for propagation of these lines were obtained from Harlan/Envigo. All alleles used in this study have been backcrossed for numerous generations to the ICR background, although because of intercrosses this was not rigorously controlled or quantified. All experiments with animals complied with National Institutes of Health guidelines and were reviewed and approved by the Medical University of South Carolina Institutional Animal Care and Use Committee. Wild-type ICR mice used for propagation of these lines were obtained from Harlan/Envigo.

24-hour fecal collection. 2.5-week-old animals were individually housed in a single mouse metabolic cage (Tecniplast) for 24 hours. Feces collected in a collection funnel were dried and measured for their dry weight.

Embryonic gut slice collagen gel explant culture. Tomato^{+} mutant and their littermate control embryos were dissected in PBS. To ensure similar stages of development between litters, E10.5 tissues were only used if the midgut was 1.0-1.4mm, and for E11.5 tissue if the proximal midgut segment was 1.6-2.0mm. Tissues were sectioned with a Vibratome 1000 microtome as described in Figure 5 – figure supplement 1. Each 200μm section was placed in a culture medium droplet on a Petri dish and maintained in caudal-rostral order. Each embryonic gut slice was placed onto a collagen bed and mounted with additional collagen solution, then culture media with or without growth factor was added to the Petri dish to fully submerge the collagen gel domes. After 3 days, Petri dishes containing the collagen domes were fixed in 4% PFA then processed for imaging.

An expanded description of these and all additional procedures is provided in the Supplemental Materials.

References

Aldinger, K. A., Sokoloff, G., Rosenberg, D. M., Palmer, A. A., & Millen, K. J. (2009). Genetic variation and population substructure in outbred CD-1 mice: implications for genome-wide association studies. *PLoS One, 4*(3), e4729. doi: 10.1371/journal.pone.0004729

Anderson RB, N. D., Young HM. (2000). Neural Crest and the Development of the Enteric Nervous SystemMadame Curie Bioscience Database. Austin (TX): Landes Bioscience.

Baker, C. V., & Bronner-Fraser, M. (2001). Vertebrate cranial placodes I. Embryonic induction. *Dev Biol, 232*(1), 1-61. doi: 10.1006/dbio.2001.0156

Barald, K. F., & Kelley, M. W. (2004). From placode to polarization: new tunes in inner ear development. *Development, 131*(17), 4119-4130. doi: 10.1242/dev.01339

Barlow, A., de Graaff, E., & Pachnis, V. (2003). Enteric nervous system progenitors are coordinately controlled by the G protein-coupled receptor EDNRB and the receptor tyrosine kinase RET. *Neuron, 40*(5), 905-916. doi: 10.1016/s0896-6273(03)00730-x

Baynash, A. G., Hosoda, K., Giaid, A., Richardson, J. A., Emoto, N., Hammer, R. E., & Yanagisawa, M. (1994). Interaction of endothelin-3 with endothelin-B receptor is essential for development of epidermal melanocytes and enteric neurons. *Cell, 79*(7), 1277-1285. doi: 0092-8674(94)90018-3

Cantrell, V. A., Owens, S. E., Chandler, R. L., Airey, D. C., Bradley, K. M., Smith, J. R., & Southard-Smith, E. M. (2004). Interactions between Sox10 and EdnrB modulate penetrance and severity of aganglionosis in the Sox10Dom mouse model of Hirschsprung disease. *Hum Mol Genet, 13*(19), 2289-2301. doi: 10.1093/hmg/ddh243

Carrasquillo, M. M., McCallion, A. S., Puffenberger, E. G., Kashuk, C. S., Nouri, N., & Chakravarti, A. (2002). Genome-wide association study and mouse model identify interaction between RET and EDNRB pathways in Hirschsprung disease. *Nat Genet, 32*(2), 237-244. doi: 10.1038/ng998

Chen, M. K., Hsu, J. L., & Hung, M. C. (2020). Nuclear receptor tyrosine kinase transport and functions in cancer. *Adv Cancer Res, 147*, 59-107. doi: 10.1016/bs.acr.2020.04.010

Chen, M. K., & Hung, M. C. (2015). Proteolytic cleavage, trafficking, and functions of nuclear receptor tyrosine kinases. *FEBS J, 282*(19), 3693-3721. doi: 10.1111/febs.13342

Costa, M., Furness, J. B., Pompolo, S., Brookes, S. J., Bornstein, J. C., Bredt, D. S., & Snyder, S. H. (1992). Projections and chemical coding of neurons with immunoreactivity for nitric oxide synthase in the guinea-pig small intestine. *Neurosci Lett, 148*(1-2), 121-125.

D'Amico-Martel, A., & Noden, D. M. (1983). Contributions of placodal and neural crest cells to avian cranial peripheral ganglia. *Am J Anat, 166*(4), 445-468. doi: 10.1002/aja.1001660406

Dang, R., Torigoe, D., Suzuki, S., Kikkawa, Y., Moritoh, K., Sasaki, N., & Agui, T. (2011). Genetic background strongly modifies the severity of symptoms of Hirschsprung disease, but not hearing loss in rats carrying Ednrb(sl) mutations. *PLoS One, 6*(9), e24086. doi: 10.1371/journal.pone.0024086

Danielian, P. S., Muccino, D., Rowitch, D. H., Michael, S. K., & McMahon, A. P. (1998). Modification of gene activity in mouse embryos in utero by a tamoxifen-inducible form of Cre recombinase. *Curr Biol, 8*(24), 1323-1326. doi: S0960-9822(07)00562-3

Durbec, P. L., Larsson-Blomberg, L. B., Schuchardt, A., Costantini, F., & Pachnis, V. (1996). Common origin and developmental dependence on c-ret of subsets of enteric and sympathetic neuroblasts. *Development, 122*(1), 349-358.

Fuchs, S., Amiel, J., Claudel, S., Lyonnet, S., Corvol, P., & Pinet, F. (2001). Functional characterization of three mutations of the endothelin B receptor gene in patients with Hirschsprung's disease: evidence for selective loss of Gi coupling. *Mol Med, 7*(2), 115-124.

Furness, J. (2006). *The Enteric Nervous System*: Blackwell.

Gong, S., Doughty, M., Harbaugh, C. R., Cummins, A., Hatten, M. E., Heintz, N., & Gerfen, C. R. (2007). Targeting Cre recombinase to specific neuron populations with bacterial artificial chromosome constructs. *J Neurosci, 27*(37), 9817-9823. doi: 10.1523/JNEUROSCI.2707-07.2007

Goto, A., Sumiyama, K., Kamioka, Y., Nakasyo, E., Ito, K., Iwasaki, M., . . . Matsuda, M. (2013). GDNF and endothelin 3 regulate migration of enteric neural crest-derived cells via protein kinase A and Rac1. *J Neurosci, 33*(11), 4901-4912. doi: 10.1523/JNEUROSCI.4828-12.2013

Grantcharova, E., Reusch, H. P., Grossmann, S., Eichhorst, J., Krell, H. W., Beyermann, M., . . . Oksche, A. (2006). N-terminal proteolysis of the endothelin B receptor abolishes its ability to induce EGF receptor transactivation and contractile protein expression in vascular smooth muscle cells. *Arterioscler Thromb Vasc Biol, 26*(6), 1288-1296. doi: 10.1161/01.ATV.0000220377.51354.30

Guthrie, S., & Lumsden, A. (1994). Collagen Gel Coculture of Neural Tissue. *Neuroprotocols, 4*(2), 116-120. doi: https://doi.org/10.1006/ncmn.1994.1014

Harun-Or-Rashid, M., Konjusha, D., Galindo-Romero, C., & Hallbook, F. (2016). Endothelin B Receptors on Primary Chicken Muller Cells and the Human MIO-M1 Muller Cell Line Activate ERK Signaling via Transactivation of Epidermal Growth Factor Receptors. *PLoS One, 11*(12), e0167778. doi: 10.1371/journal.pone.0167778

Hosoda, K., Hammer, R. E., Richardson, J. A., Baynash, A. G., Cheung, J. C., Giaid, A., & Yanagisawa, M. (1994). Targeted and natural (piebald-lethal) mutations of endothelin-B receptor gene produce megacolon associated with spotted coat color in mice. *Cell, 79*(7), 1267-1276. doi: 0092-8674(94)90017-5

Kapur, R. P. (2000). Colonization of the murine hindgut by sacral crest-derived neural precursors: experimental support for an evolutionarily conserved model. *Dev Biol, 227*(1), 146-155. doi: 10.1006/dbio.2000.9886

Keast, J. R. (1995). Visualization and immunohistochemical characterization of sympathetic and parasympathetic neurons in the male rat major pelvic ganglion. *Neuroscience, 66*(3), 655-662.

Kilpatrick, L. E., & Hill, S. J. (2021). Transactivation of G protein-coupled receptors (GPCRs) and receptor tyrosine kinases (RTKs): Recent insights using luminescence and fluorescence technologies. *Curr Opin Endocr Metab Res, 16*, 102-112. doi: 10.1016/j.coemr.2020.10.003

Kuruvilla, R., Zweifel, L. S., Glebova, N. O., Lonze, B. E., Valdez, G., Ye, H., & Ginty, D. D. (2004). A neurotrophin signaling cascade coordinates sympathetic neuron development through differential control of TrkA

trafficking and retrograde signaling. *Cell, 118*(2), 243-255. doi: 10.1016/j.cell.2004.06.021 S0092867404005847 [pii]

Ladher, R. K., O'Neill, P., & Begbie, J. (2010). From shared lineage to distinct functions: the development of the inner ear and epibranchial placodes. *Development, 137*(11), 1777-1785. doi: 10.1242/dev.040055

Lake, J. I., & Heuckeroth, R. O. (2013). Enteric nervous system development: migration, differentiation, and disease. *Am J Physiol Gastrointest Liver Physiol, 305*(1), G1-24. doi: 10.1152/ajpgi.00452.2012

Le Douarin, N. M. (1982). *The Neural Crest*. Cambridge: Cambridge University Press.

Luo, W., Wickramasinghe, S. R., Savitt, J. M., Griffin, J. W., Dawson, T. M., & Ginty, D. D. (2007). A hierarchical NGF signaling cascade controls Ret-dependent and Ret-independent events during development of nonpeptidergic DRG neurons. *Neuron, 54*(5), 739-754. doi: 10.1016/j.neuron.2007.04.027

Madisen, L., Zwingman, T. A., Sunkin, S. M., Oh, S. W., Zariwala, H. A., Gu, H., . . . Zeng, H. (2010). A robust and high-throughput Cre reporting and characterization system for the whole mouse brain. *Nat Neurosci, 13*(1), 133-140. doi: 10.1038/nn.2467

Makita, T., Sucov, H. M., Gariepy, C. E., Yanagisawa, M., & Ginty, D. D. (2008). Endothelins are vascular-derived axonal guidance cues for developing sympathetic neurons. *Nature, 452*(7188), 759-763. doi: nature06859 10.1038/nature06859

McCallion, A. S., Stames, E., Conlon, R. A., & Chakravarti, A. (2003). Phenotype variation in two-locus mouse models of Hirschsprung disease: tissue-specific interaction between Ret and Ednrb. *Proc Natl Acad Sci U S A, 100*(4), 1826-1831. doi: 10.1073/pnas.0337540100

Mitchell, P. J., Timmons, P. M., Hebert, J. M., Rigby, P. W., & Tjian, R. (1991). Transcription factor AP-2 is expressed in neural crest cell lineages during mouse embryogenesis. *Genes Dev, 5*(1), 105-119.

Mueller, J. L., & Goldstein, A. M. (2022). The science of Hirschsprung disease: What we know and where we are headed. *Semin Pediatr Surg, 31*(2), 151157. doi: 10.1016/j.sempedsurg.2022.151157

Nagy, N., & Goldstein, A. M. (2017). Enteric nervous system development: A crest cell's journey from neural tube to colon. *Semin Cell Dev Biol, 66*, 94-106. doi: 10.1016/j.semcdb.2017.01.006

Ohyama, T., & Groves, A. K. (2004). Generation of Pax2-Cre mice by modification of a Pax2 bacterial artificial chromosome. *Genesis, 38*(4), 195-199. doi: 10.1002/gene.20017

Parisi, M. A., & Kapur, R. P. (2000). Genetics of Hirschsprung disease. *Curr Opin Pediatr, 12*(6), 610-617.

Prigge, J. R., Wiley, J. A., Talago, E. A., Young, E. M., Johns, L. L., Kundert, J. A., . . . Schmidt, E. E. (2013). Nuclear double-fluorescent reporter for in vivo and ex vivo analyses of biological transitions in mouse nuclei. *Mamm Genome*. doi: 10.1007/s00335-013-9469-8

Rattner, A., Yu, H., Williams, J., Smallwood, P. M., & Nathans, J. (2013). Endothelin-2 signaling in the neural retina promotes the endothelial tip cell state and inhibits angiogenesis. *Proc Natl Acad Sci U S A, 110*(40), E3830-3839. doi: 10.1073/pnas.1315509110

Sanchez, M. P., Silos-Santiago, I., Frisen, J., He, B., Lira, S. A., & Barbacid, M. (1996). Renal agenesis and the absence of enteric neurons in mice lacking GDNF. *Nature, 382*(6586), 70-73. doi: 10.1038/382070a0

Sarna, S. K. (2010). *Colonic Motility: From Bench Side to Bedside* (2011/04/01 ed.). San Rafael (CA): Morgan & Claypool Life Sciences.

Schuchardt, A., D'Agati, V., Larsson-Blomberg, L., Costantini, F., & Pachnis, V. (1994). Defects in the kidney and enteric nervous system of mice lacking the tyrosine kinase receptor Ret. *Nature, 367*(6461), 380-383. doi: 10.1038/367380a0

Serbedzija, G. N., Bronner-Fraser, M., & Fraser, S. E. (1989). A vital dye analysis of the timing and pathways of avian trunk neural crest cell migration. *Development, 106*(4), 809-816.

Soriano, P. (1999). Generalized lacZ expression with the ROSA26 Cre reporter strain. *Nat Genet, 21*(1), 70-71. doi: 10.1038/5007

Southard-Smith, E. M., Kos, L., & Pavan, W. J. (1998). Sox10 mutation disrupts neural crest development in Dom Hirschsprung mouse model. *Nat Genet, 18*(1), 60-64. doi: 10.1038/ng0198-60

Srinivas, S., Watanabe, T., Lin, C. S., William, C. M., Tanabe, Y., Jessell, T. M., & Costantini, F. (2001). Cre reporter strains produced by targeted insertion of EYFP and ECFP into the ROSA26 locus. *BMC Dev Biol, 1*, 4.

Tan, J. V. S., Duron, A., Sucov, H. M., & Makita, T. (2023). Placode and neural crest origins of congenital deafness in mouse models of Waardenburg-Shah syndrome. *bioRxiv*, 2023.2010.2027.564370. doi: 10.1101/2023.10.27.564370

Theveneau, E., & Mayor, R. (2012). Neural crest delamination and migration: from epithelium-to-mesenchyme transition to collective cell migration. *Dev Biol, 366*(1), 34-54. doi: 10.1016/j.ydbio.2011.12.041

Timmermans, J. P., Barbiers, M., Scheuermann, D. W., Bogers, J. J., Adriaensen, D., Fekete, E., . . . De Groodt-Lasseel, M. H. (1994). Nitric oxide synthase immunoreactivity in the enteric nervous system of the developing human digestive tract. *Cell Tissue Res, 275*(2), 235-245.

Tsuchioka, M., Takebayashi, M., Hisaoka, K., Maeda, N., & Nakata, Y. (2008). Serotonin (5-HT) induces glial cell line-derived neurotrophic factor (GDNF) mRNA expression via the transactivation of fibroblast growth factor receptor 2 (FGFR2) in rat C6 glioma cells. *J Neurochem, 106*(1), 244-257. doi: 10.1111/j.1471-4159.2008.05357.x

Yamauchi, Y., Abe, K., Mantani, A., Hitoshi, Y., Suzuki, M., Osuzu, F., . . . Yamamura, K. (1999). A novel transgenic technique that allows specific marking of the neural crest cell lineage in mice. *Dev Biol, 212*(1), 191-203. doi: 10.1006/dbio.1999.9323

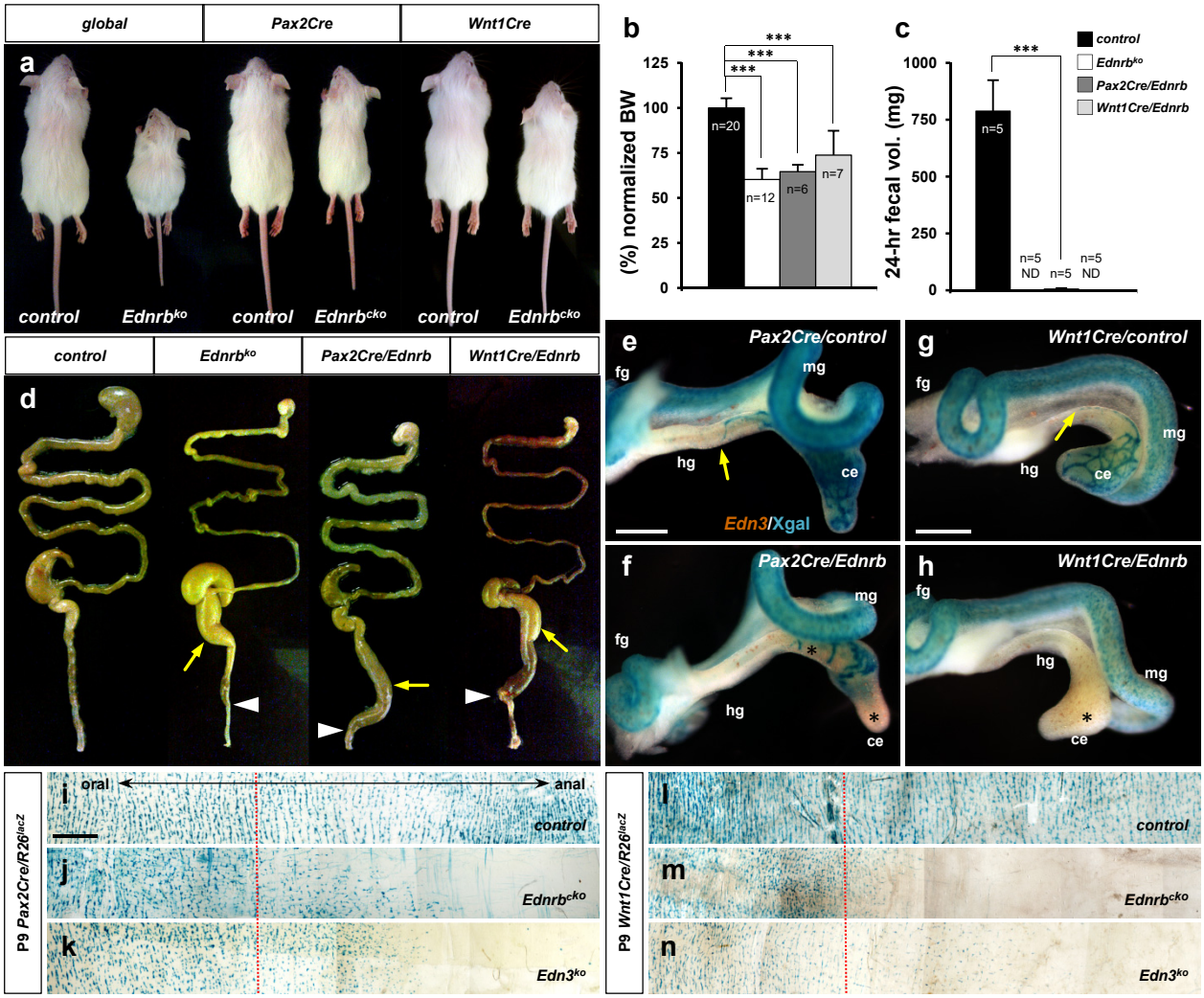

Figure 1. *Pax2Cre/Ednrb* mutants mice exhibit impaired colonic peristalsis. (a) External appearances of 3-week-old global *Ednrb* (left), *Pax2Cre/Ednrb* (middle) and *Wnt1Cre/Ednrb* (right) mutant mice compared to their littermate controls. **(b,c)** Compiled representation of normalized body weights (b) and 24-hour fecal elimination (c) from P18 mice of indicated genotypes. Error bars; mean±s.e.m. ND; not detected. P-value: ****p<0.001*. **(d)** External appearances of P18 guts from the indicated genotypes. Arrows indicate distention of colon. Arrowheads point to constriction in the distal colon. **(e-h)** Wholemount preparations of E12.5 guts isolated from *Pax2Cre/Ednrb/R26^{lacZ}* (f), *Wnt1Cre/Ednrb/R26^{lacZ}* (h) mutant embryos and their littermate controls (e and g, respectively) stained with Xgal and labeled by *in situ* hybridization for *Edn3* expression (brown). Yellow arrows denote *Pax2Cre*-labeled (e) or *Wnt1Cre*-labeled (g) Xgal$^+$ cells reaching the proximal-distal colon junction in control embryos, whereas *Ednrb*-deficient *Pax2Cre*-labeled cells (f) or *Wnt1Cre*-labeled cells (h) are deficient in caudal migration (asterisks) at the time when the *Edn3* gene is normally expressed. **(i-n)** Wholemount preparations of P9 distal colons isolated from *Pax2Cre/Ednrb* (j), *Edn3* null (k), and control (i) mice, and *Wnt1Cre/Ednrb* (m), global *Edn3* null (n), and control (l) mice stained with Xgal to visualize lineage-labeled cells. Dotted lines indicate the junction between supply by the superior mesenteric and inferior mesenteric arteries, the latter being the vascular source for the distal colon. Abbreviations: ce, cecum; fg, foregut; hg, hindgut; mg, midgut. Scale bars, 500µm (e-f, g-h), 1000µm (i-n).

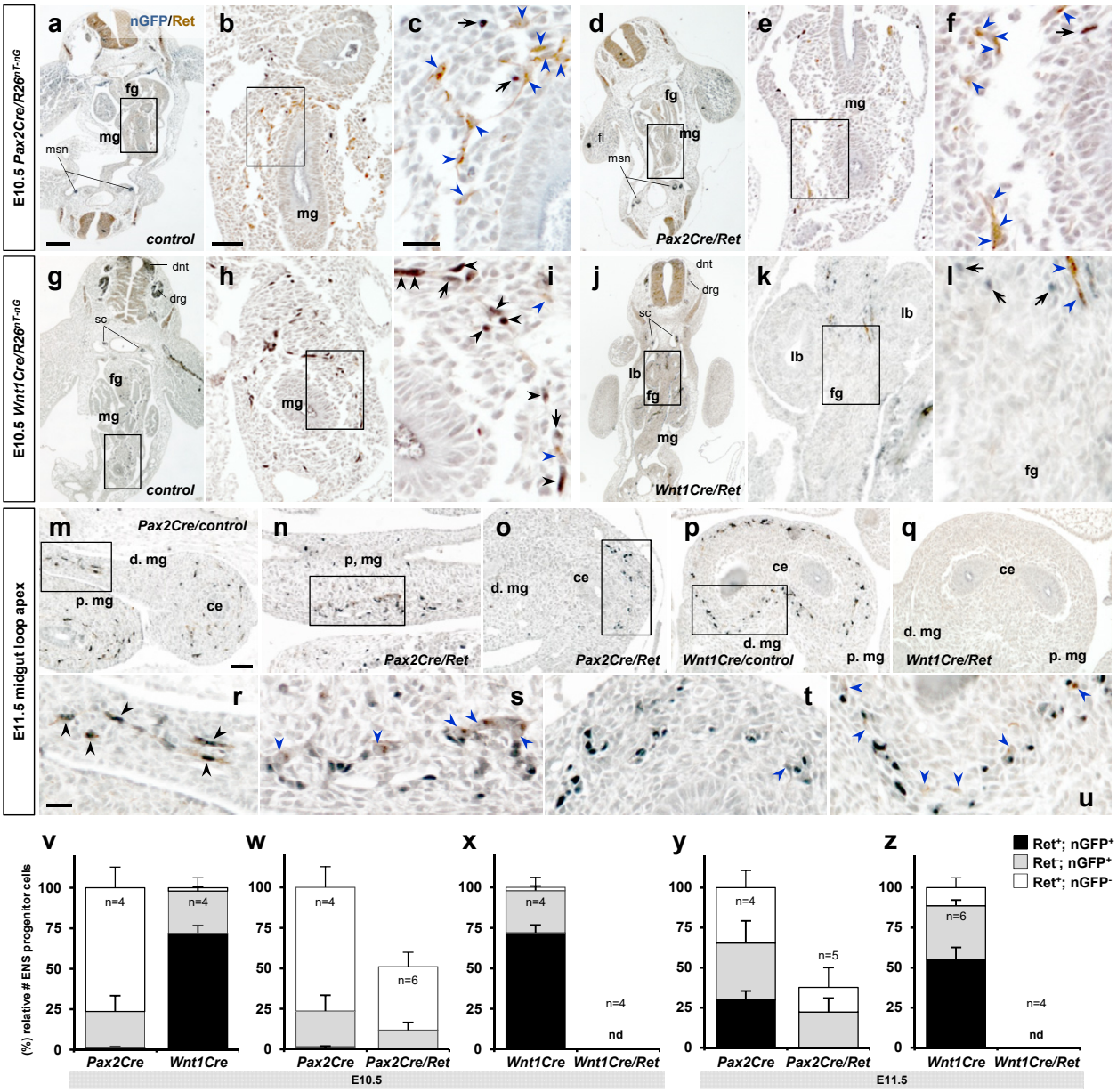

Figure 2. Developmental transition of Ret expression in migratory ENS progenitor cells. (a-u) Histological sections prepared from E10.5 *Pax2Cre/Ret/R26$^{nT\text{-}nG}$* mutant (d-f), *Wnt1Cre/Ret/R26$^{nT\text{-}nG}$* mutant (j-l), and their littermate controls (a-c, and g-l, respectively), and E11.5 *Pax2Cre/Ret/R26$^{nT\text{-}nG}$* mutant (n-o), *Wnt1Cre/Ret/R26$^{nT\text{-}nG}$* mutant (q), and their littermate control embryos (m and p, respectively) stained for nuclear-GFP (blue) and Ret (brown). Magnified views of the bracketed areas (midgut) in a, d, g and j are shown in b, e, h and k, respectively. Magnified views of the bracketed areas in b, e, h and k are shown in c, f, I and l, respectively. Magnified views of the bracketed areas in m-p are shown in r-u, respectively. Black arrows denotes lineage marker nGFP$^+$ nuclei with no Ret stain, black arrowheads denoted cells that are positive for both nuclear GFP and Ret, and blue arrowheads denote non-Cre (nGFP$^-$) Ret$^+$ cells along the gut walls. **(v-z)** Compiled representations of relative fractions of Ret$^+$,nGFP$^+$ (black); Ret$^-$,nGFP$^+$ (grey); and Ret$^+$,nGFP$^-$ (white) ENS progenitor cells comparing (v) E10.5 midgut areas of *Pax2Cre/R26$^{nT\text{-}nG}$* (n=4; total 228 cells) and *Wnt1Cre/R26$^{nT\text{-}nG}$* (n=4; total 185 cells) embryos, (w) E10.5 midgut areas of *Pax2Cre/Ret/R26$^{nT\text{-}nG}$* mutants (n=6, total 196 cells) and littermate control embryos, (x) E10.5 midgut areas of *Wnt1Cre/Ret/R26$^{nT\text{-}nG}$* mutants (n=4, no nGFP$^+$ or Ret$^+$ cell was found) and littermate control embryos, (y) E11.5 midgut loop apex areas of *Pax2Cre/Ret/R26$^{nT\text{-}nG}$* mutants (n=5, total 900 cells) and littermate control embryos (n=4, total 1068 cells), and (z) E11.5 midgut loop apex areas of *WntCre/Ret/R26$^{nT\text{-}nG}$* mutants (n=4, no nGFP$^+$ or Ret$^+$ cell was found) and littermate control embryos (n=6, total 1765 cells). Data in v are the control mouse groups in w and x, shown together for easier comparison. The Ret$^-$,nGFP$^-$ (double negative) cell population was not included in this analysis. nd=not detected. Abbreviations: dnt, dorsal neural tube; drg, dorsal root ganglia; msn, mesonephros; sc, sympathetic chain ganglia. Scale bars, 200µm (a, d, g, j), 50µm (b, e, h, k, m-q), 20µm (c, f, i, l, r-u).

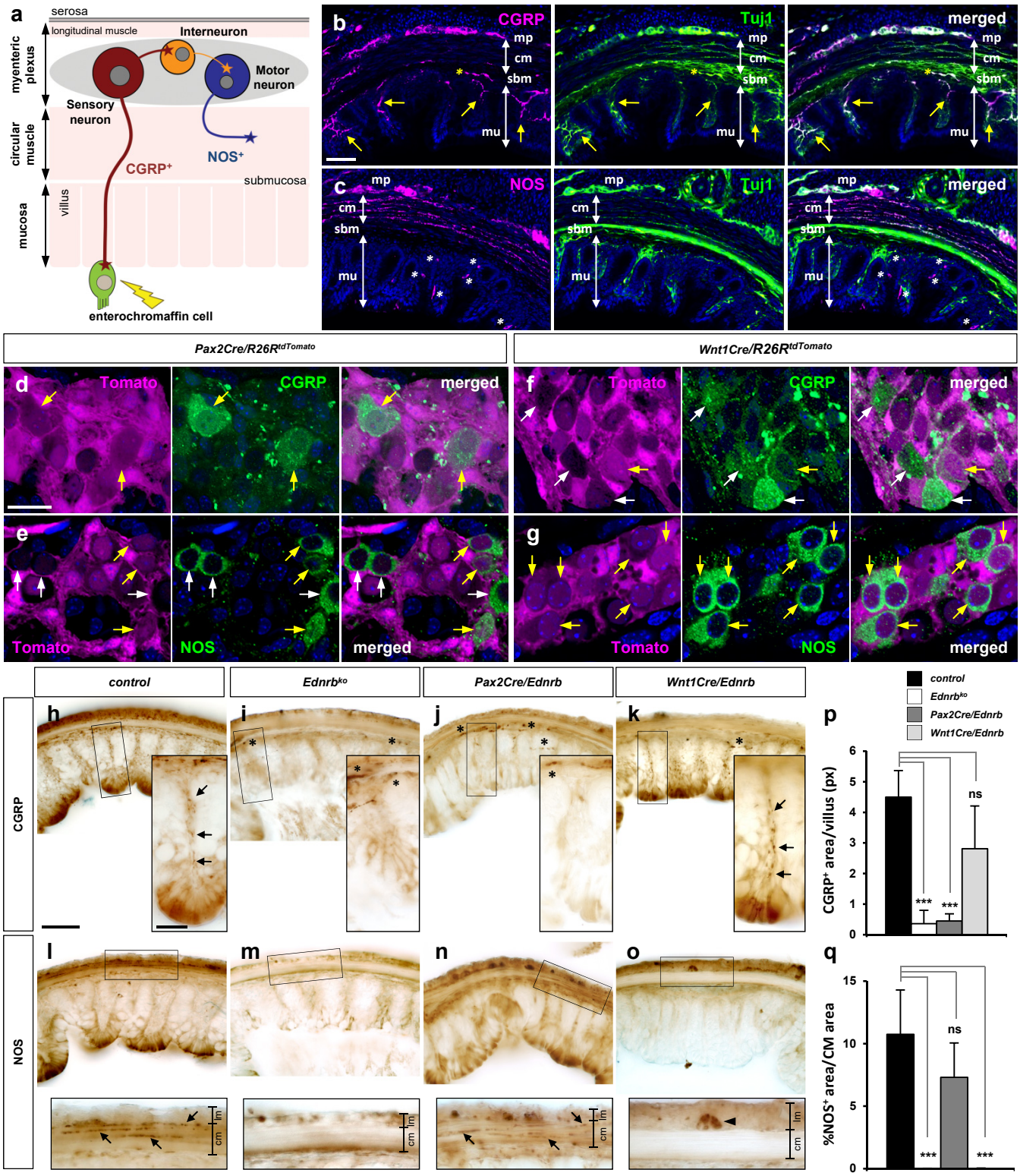
a
serosa
longitudinal muscle
Interneuron
myenteric plexus
Motor neuron
Sensory neuron
circular muscle
NOS+
CGRP+
submucosa
mucosa
villus
enterochromaffin cell
b
CGRP
Tuj1
merged
mp
cm
sbm
mu
c
NOS
Pax2Cre/R26RtdTomato
Wnt1Cre/R26RtdTomato
d
Tomato
e
f
g
control
Ednrbko
Pax2Cre/Ednrb
Wnt1Cre/Ednrb
h
i
j
k
l
m
n
o
lm
p
q
ns
***
CGRP+ area/villus (px)
%NOS+ area/CM area

Figure 3. Mechanosensory fate of *Pax2Cre* lineage and selective loss of CGRP$^+$ myenteric mechanosensory axons in *Pax2Cre/Ednrb* mutant distal colon. (a) Schematic illustration of neuronal subtypes in the colonic myenteric ganglia and their endorgans. Mechanosensory neurons (red) extend their peripheral axons to the mechanosensory (enterochromaffin) cells while their other axons synapse to interneurons (orange). Motor neurons (blue) innervate the colonic circular muscle to generate colonic peristalsis. **(b-c)** Confocal images of transverse sections of the distal colon co-immunostained for CGRP and Tuj1 (b) or NOS and Tuj1 (c) show selective label of sensory and motor axons by CGRP (b) and NOS (c), respectively. Yellow arrows in b denote CGRP$^+$ axons that project through each villus to reach enteric epithelium. Yellow asterisks in b indicate CGRP$^+$ axons from pelvic ganglia along the submucosal layer. White asterisks in c point to NOS-reactive non-neuronal epithelial cells of the mucosa. **(d-g)** Confocal images of the myenteric ganglia of P9 distal colons isolated from *Pax2Cre/R26^{tdTomato}* (d-e) and *Wnt1Cre/R26^{tdTomato}* (f-g) mice immunostained for CGRP (d, f) and NOS (e, g). Low magnification views from which these images were taken are shown in Supplemental Figure S4. Compared to b and c, this wholemount preparation emphasizes cell bodies in the myenteric plexus rather than axon projections. Yellow arrows point to lineage marker-positive CGRP$^+$ or NOS$^+$ neurons, whereas white arrows indicate lineage marker-negative CGRP$^+$ or NOS$^+$ neurons of the myenteric ganglia. **(h-o)** Serial transverse vibratome sections of the transition areas (see Supplemental Figure S6c, 6h) of the distal colons isolated from P9 control (h, l), global *Ednrb* (i, m), *Pax2Cre/Ednrb* (j, n) and *Wnt1Cre/Ednrb* (k, o) mutants immunostained for CGRP (h-k) or NOS (l-o). Magnified views of bracketed areas are shown in the insets. Arrows in h and k denote CGRP$^+$ axonal projections toward mucosal epithelium in a single villus. Arrows in l and n denote NOS$^+$ axonal projections perforating throughout the circular muscle layer. Arrowhead in o indicates a NOS$^+$ presumed myenteric interneuron (because it lacks motor axons in the circular muscle layer) of *Wnt1Cre/Ednrb* mutant colon. **(p)** Complied representation of the average pixel values of CGRP$^+$ axon area per single villus. **(q)** Complied representation of the average fraction of NOS$^+$ axon area in the circular muscle area. Analysis includes 24 villi from 8 distal colon sections per genotype (four controls, two *Ednrb*, three *Pax2Cre/Ednrb* and three *Wnt1Cre/Ednrb* mutants). P-values: ****p<0.001*, ns=not significant. Error bars, mean±s.e.m. Scale bars, 50μm (b-c, h-o), 20μm (d-g, h-o insets). Abbreviations: cm, circular muscle; lm, longitudinal muscle; mp, myenteric plexus; mu, mucosa; sbm, submucosa.

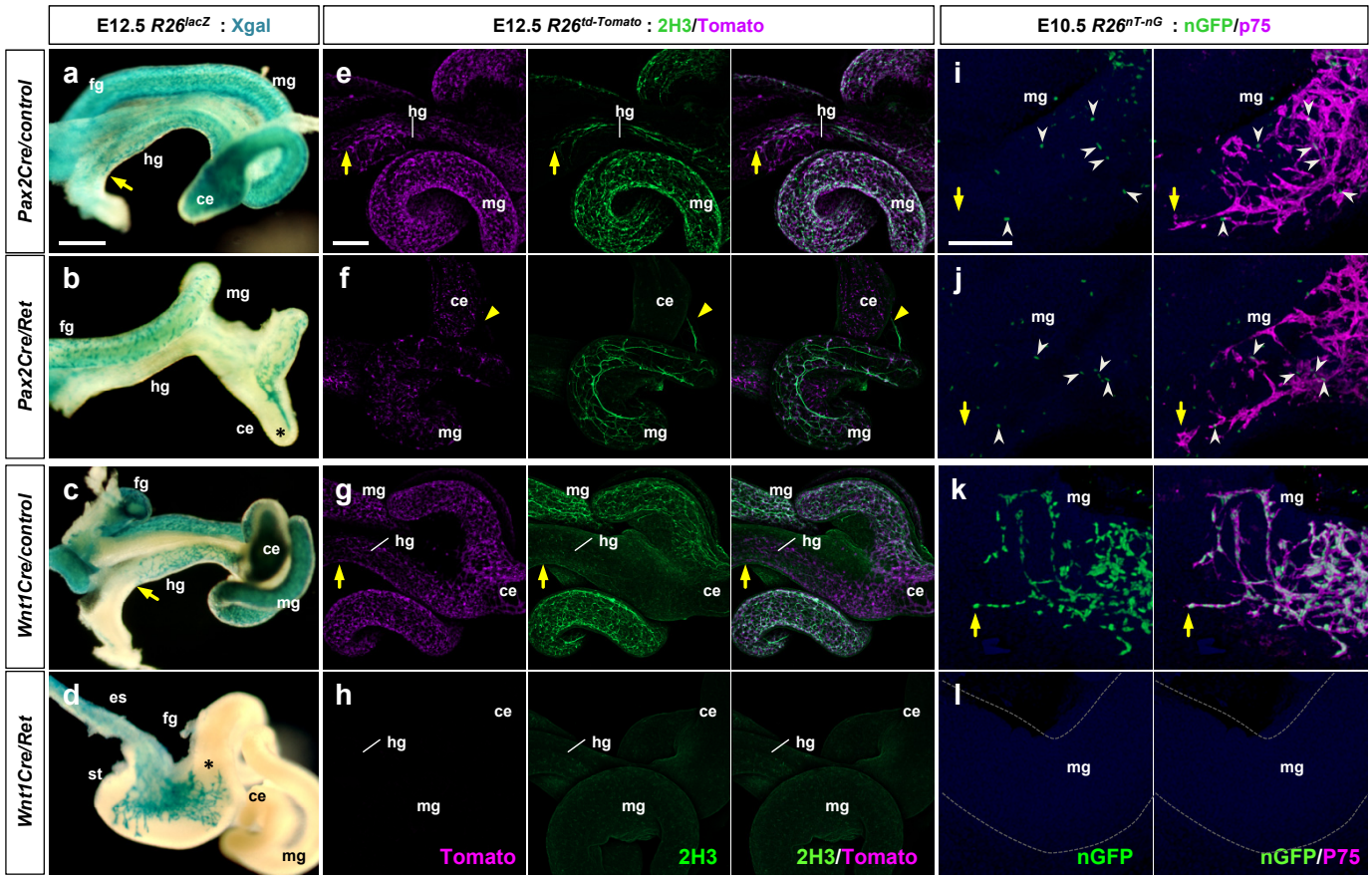

Figure 4. Pax2Cre-specific deletion of *Ret* results in defective ENS progenitor migration and differentiation. (a-d) Wholemount preparations of E12.5 guts isolated from *Pax2Cre/Ret/R26*^{lacZ} (b), *Wnt1Cre/Ret/R26*^{lacZ} (d) mutant embryos and their littermate controls (a and c, respectively) stained with Xgal (blue). Arrows denote the wavefronts of lineage-labeled cells in the hindguts of the controls. Asterisks denote halted migration of *Ret*-deficient *Pax2Cre*-labeled cells at the cecum (b) and of *Ret*-deficient *Wnt1Cre*-labeled cells at the caudal end of the stomach (d). **(e-h)** Wholemount preparations of E12.5 guts isolated from *Pax2Cre/Ret/R26*$^{td\text{-}Tomato}$ (f), *Wnt1Cre/Ret/R26*$^{td\text{-}Tomato}$ (h) mutant embryos and their littermate controls (e and g, respectively) stained for neuronal 2H3 (green). Arrows denote the wavefronts of lineage-labeled cells in the hindguts of the control embryos. Arrowheads denote halted migration of *Ret*-deficient *Pax2Cre*-labeled cells at the cecum (f). **(i-l)** Wholemount preparations of E10.5 guts isolated from *Pax2Cre/Ret/R26*$^{nT\text{-}nG}$(j), *Wnt1Cre/Ret/R26*$^{nT\text{-}nG}$ (l) mutant embryos and their littermate controls (i and k, respectively) stained for nuclear-GFP (green) and ENS progenitor marker p75 (magenta). Arrows denote the wavefronts of lineage-labeled cells in the midguts. Arrowheads denote p75^{+} *Pax2Cre*-labeled cells at the midgut areas (i-j). Abbreviations: es, esophagus; st, stomach. Scale bars, 500μm (a-d), 250μm (e-h), 50μm (i-l).

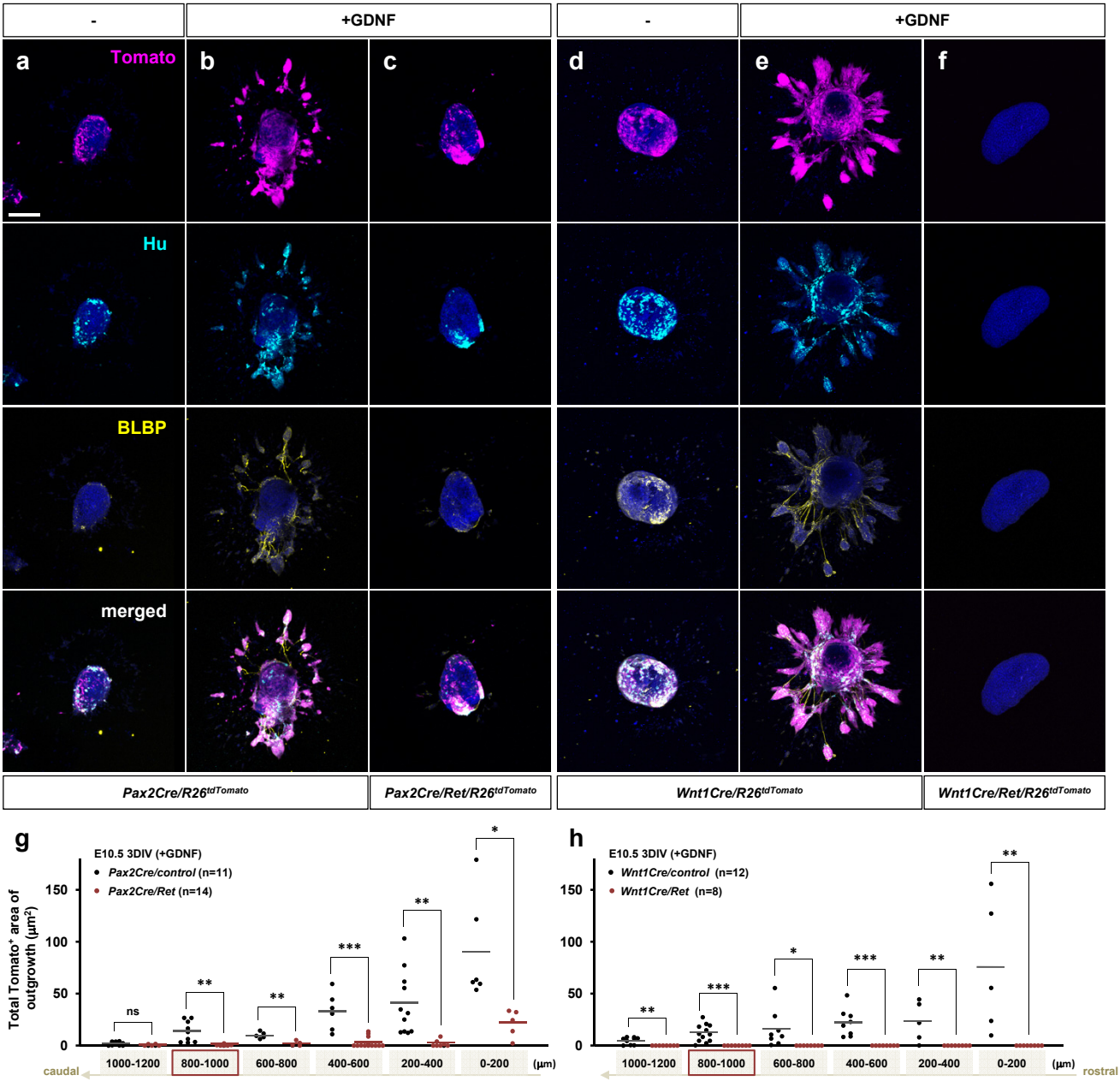

Figure 5. Defective GDNF-induced outgrowth and differentiation of *Pax2Cre/Ret* mutant ENS progenitors in vitro. (a-f) Confocal images of 200µm midgut sections isolated from an E10.5 *Pax2Cre/Ret/R26*$^{td\text{-}Tomato}$ mutant (c) and its littermate control (a-b), and a *Wnt1Cre/Ret/R26*^{tdTomato} mutant (f) and its littermate control (d-e) cultured 3 days in vitro (3DIV) in the absence (a, d) or presence of GDNF (b-c, e-f), then immunolabeled for neuronal Hu (cyan) and glial BLBP (yellow). Scale bars, 250µm. **(g)** Complied representation of the total area of outgrowth (Tomato^{+} area around the explanted gut tube) from *Pax2Cre/control* (black dots; n=11) and *Pax2Cre/Ret* mutant (red dots; n=14) embryos in the presence of GDNF. **(h)** Compiled representation of the total outgrowth area from *Wnt1Cre/control* (black dots; n=12) and *Wnt1Cre/Ret* mutant (red dots; n=8) embryos in the presence of GDNF. See Figure 5 – figure supplement 1a for rostrocaudal orientation of the midgut slice preparations. Each dot represents the outgrowth of each gut slice prepared from each embryos used for data acquisition (lost individual midgut sections are not included as data points). The images shown in a-f represent sections that are 800-1000 µm caudal to the foregut-midgut junction (as indicated by the red boxes in g-h). P-values: *$p<0.05$, **$p<0.01$, ***$p<0.001$, ns=not significant.

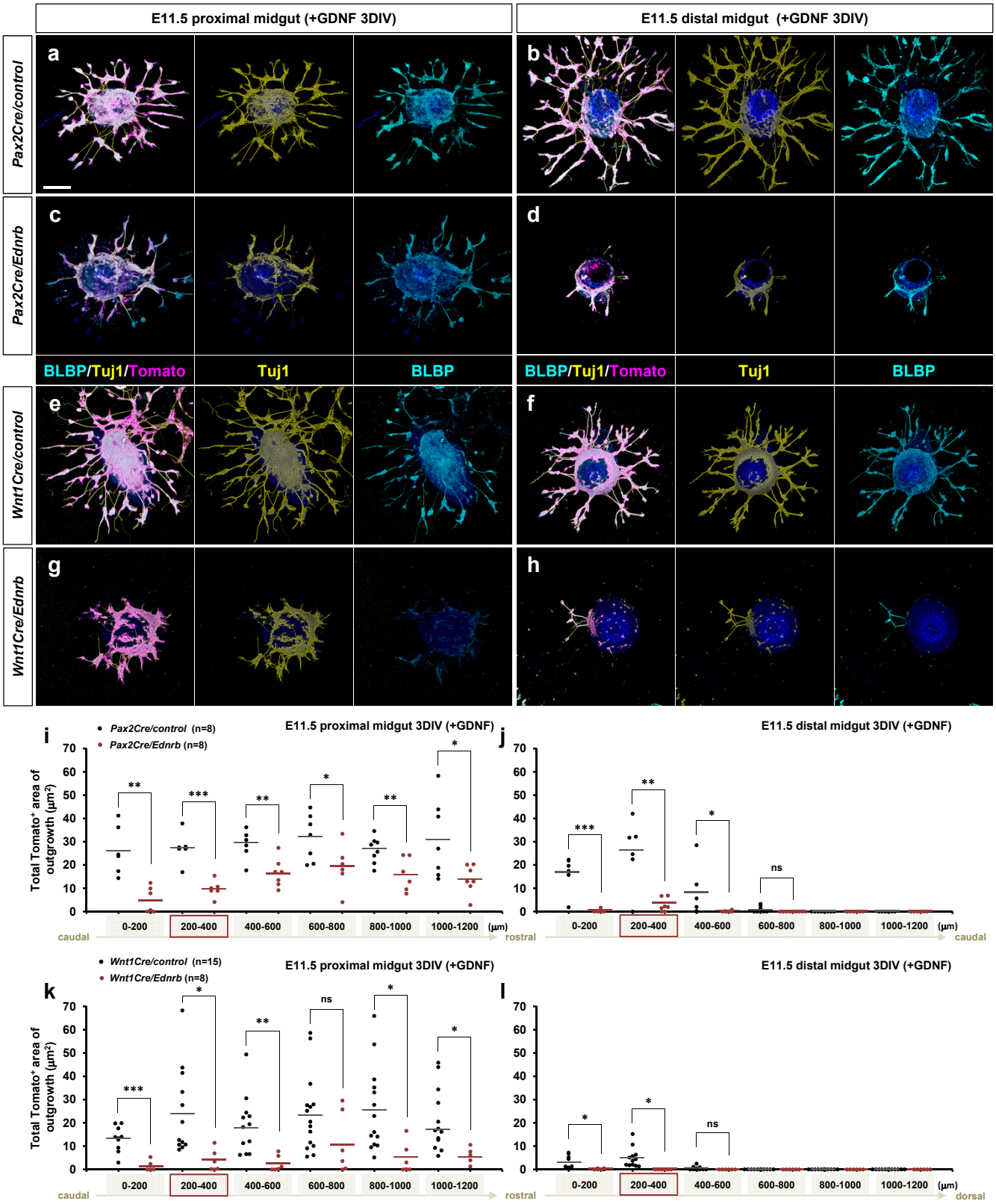
E11.5 proximal midgut (+GDNF 3DIV)
E11.5 distal midgut (+GDNF 3DIV)
Pax2Cre/control
Pax2Cre/Ednrb
Wnt1Cre/control
Wnt1Cre/Ednrb
a
b
c
d
e
f
g
h
BLBP/Tuj1/Tomato
Tuj1
BLBP
i
j
k
l
Pax2Cre/control (n=8)
Pax2Cre/Ednrb (n=8)
Wnt1Cre/control (n=15)
Wnt1Cre/Ednrb (n=8)
E11.5 proximal midgut 3DIV (+GDNF)
E11.5 distal midgut 3DIV (+GDNF)
Total Tomato+ area of outgrowth (µm²)
0-200
200-400
400-600
600-800
800-1000
1000-1200
(µm)
caudal
rostral
dorsal
ns

Figure 6. *Ednrb*-deficient ENS progenitor cells populating the migratory wavefront exhibit attenuated response to GDNF in vitro. (a-h) Confocal z-stack images of 200μm proximal (a, c, e, g) and distal midgut (b, d, f, h) sections isolated from an E11.5 *Pax2Cre/Ret/R26*$^{td\text{-}Tomato}$ mutant (c-d) and its littermate control (a-b), and a *Wnt1Cre/Ret/R26*^{tdTomato} mutant (g-h) and its littermate control (e-f) cultured 3 days in vitro (3DIV) in the presence of GDNF and then immunolabeled for neuronal Tuj1 (yellow) and glial BLBP (cyan). Scale bars, 250μm. **(i-j)** Compiled representation of the total area of outgrowth (Tomato^{+} area around the explanted gut tube) from proximal and distal midguts of *Pax2Cre/control* (black dots; n=8) and *Pax2Cre/Ret* mutant (red dots; n=8) embryos in the presence of GDNF. **(k-l)** Compiled representation of the total area of outgrowth from *Wnt1Cre/control* (black dots; n=15) and *Wnt1Cre/Ret* mutant (red dots; n=8) embryos in the presence of GDNF. See Figure 5 – figure supplement 1b for rostrocaudal orientation of the midgut slices. The proximal midgut images shown in a,c,e,g represent sections that are 200-400 μm rostral to the apex of the midgut loop; the distal midgut images shown in b,d,f,h represent sections that are 200-400 μm caudal to the apex of the midgut loop (as indicated by the red boxes in i-l). P-values: *$p<0.05$, **$p<0.01$, ***$p<0.001$, ns=not significant.

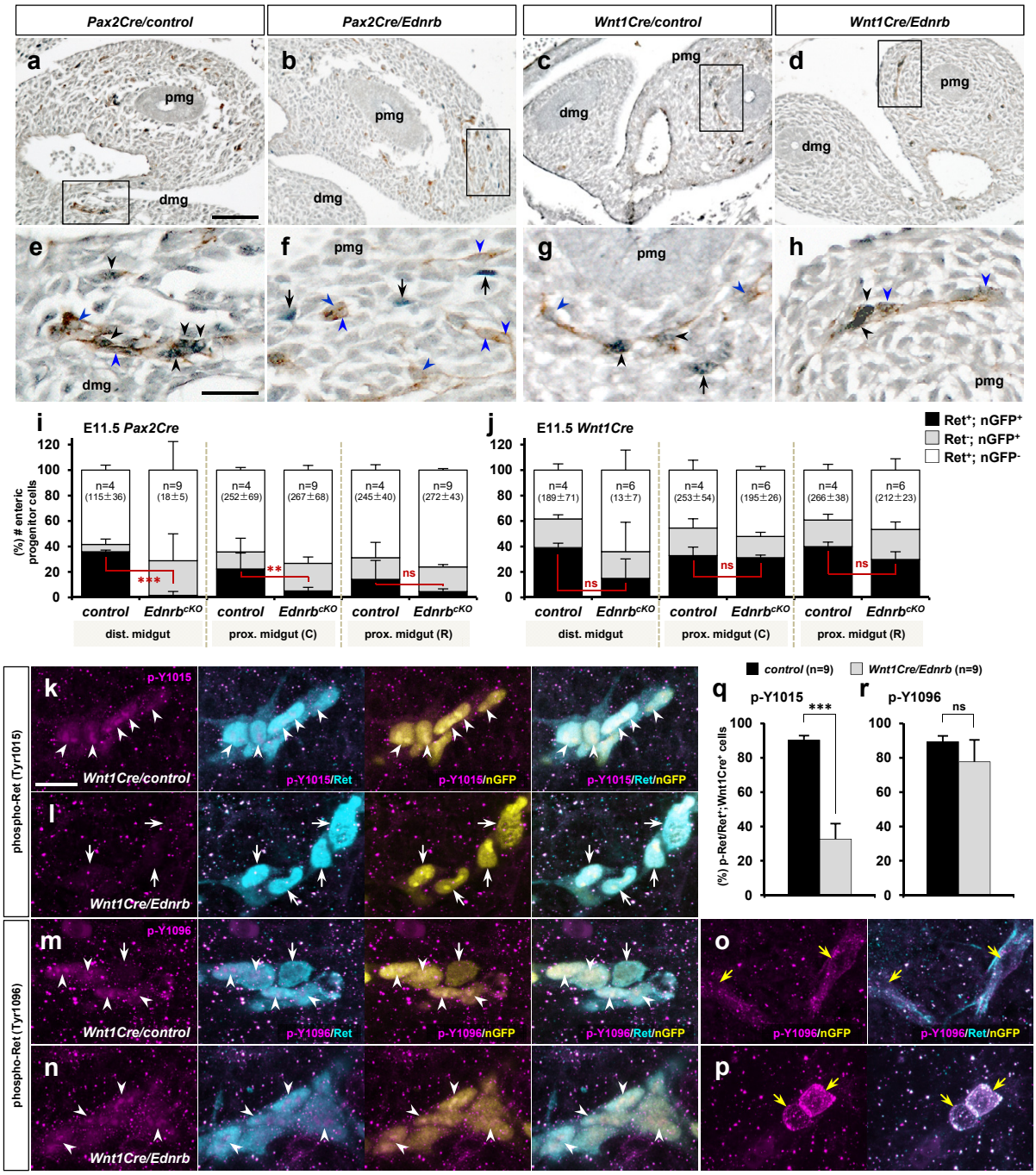

Figure 7. Lineage selective endothelin-dependent regulation of Ret in migratory ENS progenitor cells. (a-d) Histological sections showing the apex of the midgut loop of E11.5 *Pax2Cre/Ednrb/R26$^{nT\text{-}nG}$* mutant (b), *Wnt1Cre/Ednrb/R26$^{nT\text{-}nG}$* mutant (d), and their littermate control embryos (a and c, respectively) stained for nuclear-GFP (blue) and Ret (brown). Magnified views of the bracketed areas (migratory wavefronts) in a-d are shown in e-h, respectively. Abbreviations: dmg, distal midgut; pmg, proximal midgut. **(i-j)** Compiled representations of the fractions of Ret$^+$,nGFP$^+$ (black); Ret$^-$,nGFP$^+$ (grey), and Ret$^+$,nGFP$^-$ (white) ENS progenitor cells in the indicated areas of the embryos of the indicated genotype; (C) and (R) indicate caudal and rostral halves of the proximal midgut. The average total number of countable cells (labeled by either or both markers) in each gut segment is indicated in the parentheses. **(k-p)** Confocal z-stack images of wavefront cells in wholemount preparations of E11.5 guts isolated from *Wnt1Cre/Ednrb/R26$^{nT\text{-}nG}$* mutants (l,n,p) and their littermate control embryos (k,m,o) stained for nuclear-GFP (yellow), Ret (cyan), and phospho-Ret (Tyr1015) (magenta; k-l) or phospho-Ret(Tyr1096) (magenta; m-p). White arrowheads denote the presence of phosphorylated Ret in the Wnt1Cre-labeled cells, white arrows point to the absence of phosphorylated Ret in the Wnt1Cre-labeled cells, and yellow arrows denote cytoplasmic localization of phosphorylated Ret in nonlineage Ret$^+$ cells. **(q-r)** Compiled representations of phospho-Ret-(Tyr1015)$^+$ fractions (q) and phospho-Ret-(Tyr1096)$^+$ fractions (r) at the wavefront (apex of the midgut loop) in *Wnt1Cre/Ednrb* mutants (n=9; grey bars) and their littermate control embryos (n=9; black bars). P-values: **p<0.05*, ***p<0.01*, ****p<0.001*, ns=not significant. Scale bars, 50µm (a-d), 20µm (e-h, k-p).

Supplemental Materials and Methods

Postnatal distal colon preparation. Postnatal day 9 mice were anesthetized and transcardially perfused with PBS, and then the entire colon (including proximal colon) was dissected and transferred to PBS. After removing fecal materials by flushing PBS through the colon, a glass capillary tube was inserted to straighten the colon, and the colon was then fixed in an appropriate fixative at 4°C overnight. Fixatives used in this study were glutaraldehyde (0.2% glutaraldehyde, 0.4% paraformaldehyde, 2mM $MgCl_2$ in PBS) for X-gal staining, and paraformaldehyde (4% PFA in PBS) for immunofluorescence staining.

Wholemount Xgal staining. Fixed embryos, embryonic gut tissues and postnatal colon preparations were washed with detergent rinse (0.02% NP40, 0.01% sodium deoxycholate, 2mM $MgCl_2$ in PBS), and stained with Xgal staining solution (1mg/ml Xgal in 0.1M TrisHCl pH=7.4, 2mM $MgCl_2$, 0.02% NP40, 0.01% sodium deoxycholate, 5mM $K_3[Fe(CN)_6]$, 5mM $K_4[Fe(CN)_6]$ in PBS) at room temperature overnight. The colon was opened by longitudinal incision, the (inner) submucosal and mucosal layers were removed, and the outer tissue (containing circular muscle, the myenteric plexus, longitudinal muscle, and serosa) was stained. Xgal stained tissues were washed with PBS, and either or then used for *in situ* hybridization or wholemount immunostaining.

In situ hybridization. Xgal stained embryonic gut tissues were washed with PBST (1% Tween-20 in PBS), dehydrated in a methanol series ultimately to 100% methanol, then bleached in 3% H_2O_2 in methanol for 20 min at room temperature. Tissues were rehydrated in PBST, digested with 10μg/ml Proteinase K in PBST for 4 min at room temperature, and then washed in 2mg/ml glycine containing PBST. After post-fixation with 4% PFA for 10 min at room temperature, tissues were washed with PBST, equilibrated with hybridization solution (50% formamide, 5xSSC pH=4.5, 1% SDS, 50μg/ml yeast tRNA, 50μg/ml heparin), and incubated with biotin-labeled RNA probe at 70°C overnight. Tissues were then washed with hybridization solution (without yeast tRNA and heparin) three times at 70°C, three times with high stringent wash (50% Formamide, 2xSSC pH=4.5) at 65°C, and washed with PBST at room temperature. Biotinylated-probe was then detected by Streptavidin-HRP antibody followed by DAB chromogen reaction (see wholemount immunostaining below).

Frozen sections were prepared from fixed embryos that were cryoprotected in 30% sucrose in PBS followed by embedding in OCT compound. Sections were post-fixed for 10 min in 4% PFA/PBS, washed with PBST, and then acetylated in 0.25% acetic anhydride containing 0.1M triethanolamine for 5 min at room temperature. Section were equilibrated with hybridization solution (50% formamide, 5xSSC pH=4.5, 50μg/ml yeast tRNA), and incubated with DIG-labeled RNA probe at 58°C overnight. Sections were then washed with hybridization solution (without yeast tRNA) at 58°C, 2xSSC at room temperature, 2xSSC at 65°C, and followed by 0.1xSSC at 65°C. After wash with TBST (0.1% Tween-20 in TBS), DIG-labeled probe was detected by Alkaline phosphatase conjugated DIG antibody followed by NBT/BCIP reaction in NTMT (0.1M NaCl, 0.1M TrisHCl pH=9.5, 50mM $MgCl_2$, 0.1% Tween-20) with 2mM levamisole. *In situ* labeled sections were then subjected to immunofluorescence staining (see immunofluorescence staining below).

Riboprobes for *Edn3* and *Ednrb* genes are described previously (Makita, Sucov, Gariepy, Yanagisawa, & Ginty, 2008).

2-color immunohistochemistry. 5μm continuous paraffin sections prepared from the head to tail of E10.5-12.5 *Pax2Cre/Ret/R26*$^{nT\text{-}nG}$, *Pax2Cre/Ednrb/R26*$^{nT\text{-}nG}$, *WntCre/Ret/R26*$^{nT\text{-}nG}$, *Wnt1Cre/Ednrb/R26*$^{nT\text{-}nG}$, and their littermate control embryos were deparaffinized in xylene, rehydrated through an ethanol sequence, and then microwaved for 25 min in citrate buffer (10mM sodium citrate pH=6.0) for antigen retrieval. Histological slides were bleached in 3% H_2O_2 in methanol for 2 min, washed in PBST (0.1% Tween-20 in PBS), and then first incubated with chicken anti-GFP antibody (1:3000, Abcam ab13970) at 4°C overnight. After three washes with

PBST, sections were incubated with HRP conjugated anti-chicken-IgY (1:200, Jackson ImmunoResearch 703-035-155) for 2-3 hr at room temperature. GFP signal was then detected by 0.5mg/ml DAB-blue solution containing 0.05% $CoCl_2$, 0.05% $Ni(NH_4)_2(SO_4)_2$ (pH=7.2) with 0.015% H_2O_2. Nuclear-GFP immunolabeled sections were then bleached in 3% H_2O_2 in methanol for 2 min, washed in PBST (0.1% Tween-20 in PBS), and incubated with goat anti-Ret antibody (1:300, R&D Systems AF482) at 4°C overnight. After incubating with HRP-conjugated goat-IgG secondary antibody, Ret signal was detected using DAB-brown solution (0.5mg/ml DAB with 0.03% H_2O_2). Slides were washed in ddH_2O, dehydrated in an ethanol sequence followed by xylene and mounted with DPX medium.

All sections containing foregut through midgut area containing immunolabeled cells were captured as digital images using a Nikon DS-Fi1 digital camera in continuous order, and nGFP-positive, Ret-positive, and nGFP and Ret-double positive cells were counted in every third section (15μm intervals to avoid counting the same cell twice) using Fiji Image J plugin Cell Counter.

Embryonic gut slice preparation for collagen gel explant culture. Tomato$^+$ embryos from *Pax2Cre/Ret/R26$^{td\text{-}Tomato}$*, *Pax2Cre/Ednrb/R26$^{td\text{-}Tomato}$*, *WntCre/Ret/R26$^{td\text{-}Tomato}$*, *Wnt1Cre/Ednrb/R26$^{td\text{-}Tomato}$* and their littermate control embryos were collected in PBS under a fluorescence dissection scope (Nikon SMZ800), and midgut segments were dissected in PBS as described in Figure 5 – figure supplement 1. For E10.5 explants, dissected midgut segments were embedded in 6% low melt agarose in PBS, and sectioned transversely from the caudal to rostral direction using a Vibratome 1000 microtome. Each 200μm section was placed in a culture medium droplet on petri dish and these were maintained in their caudal to rostral order until explanted in collagen gel. For E11.5 explants, both proximal and distal midgut segments were separately embedded in 6% low melt agarose in PBS, sectioned in a caudal to rostral and rostral to caudal direction, respectively, and placed in culture media droplets prior to explanting in collagen gel. To ensure similar stages of development between different litters, E10.5 tissue sections were only used if the midgut was 1.0-1.4mm, and for E11.5 tissue if the proximal midgut segments was 1.6-2.0mm.

***Collagen gel explant culture*.** Rat tail collagen and collagen gel preparation were performed as previously described (Guthrie & Lumsden, 1994) with minor modifications. Briefly, rat tail collagen was prepared by dissolving 2.5mg/ml rat tail tendons in 0.5N acetic acid at 4°C for two days. The solution was then centrifuged at 12,000rpm for 1 hr at 4°C to remove debris, and the supernatant dialyzed against 0.1X Basal Eagle's Medium (BME) for 3 days at 4°C. For collagen gel explant culture, 4XBME and 7.5% sodium bicarbonate (with or without growth factor, see below) were gently placed into dialyzed rat tail collagen solution on ice to a final concentration of 1X and 0.2%, respectively. After very gentle pipetting up and down on ice, 25ul collagen drops were placed onto a Petri dish, and then flattened by gently dropping the dish onto a flat surface several times. The collagen beds were then solidified in a tissue culture incubator (5% CO_2, 37°C) for 10 min. Once the collagen beds solidified into a gel, each embryonic gut slice was placed onto a collagen bed and mounted with 40ul of freshly prepared collagen solution (1XBME, 0.2% $NaHCO_3$, with or without growth factor in dialyzed collagen), and the dish returned to the incubator for 10 min. Once the top collagen was fully solidified, culture medium with or without growth factor was added to the Petri dish to fully submerge the collagen gel domes. Gut slice explants were then cultured in 5% CO_2 at 37°C for 3 days. Culture media used was DMEM supplemented with 10% FBS, 100U/ml penicillin/streptomycin, 100μM putrescine (Sigma-Aldrich P5780), 10ng/ml progesterone (Sigma-Aldrich P7556), 200ng/ml selenious acid (Sigma-Aldrich 211176), 500μM sodium butyrate (Sigma-Aldrich B5887), 1mM sodium pyruvate (Sigma-Aldrich P2256), 5μg/ml transferrin (Sigma-Aldrich T8158), 2ng/ml triiodo-L-thyronine (T3) (Sigma-Aldrich T6397). Growth factors used were recombinant mouse GDNF (10ng/ml, Abcam ab 56286), endothelin-3 (10nM, Enzo LifeSciences ALX-155-003) and recombinant mouse NGF (10ng/ml, Sino Biological 50385-MNAC). This Edn3 concentration promotes neurite outgrowth from embryonic sympathetic and CNX ganglion explants (Makita et al., 2008) and NGF at the utilized concentration is widely used to promote growth and survival of variety of neuronal types (Kuruvilla et al., 2004). After 3 days, the Petri dishes containing

the collagen gel domes were fixed in 4% PFA for 2 hr at 4°C and washed with PBS. The explanted tissue morphology and its Tomato$^+$ cell profiles were recorded in continuous axial order under bright field and epifluorescence settings, respectively (Nikon Eclipse 80i upright microscope). The collagen domes were then gently peeled off from the Petri dish and wholemount immunofluorescence stained (see immunofluorescence staining below) for confocal imaging. Total Tomato$^+$ outgrowth area was measured from epifluorescence images acquired from a Nikon Eclipse 80i upright microscope using Fiji Image J software; binary threshold selection of the Tomato$^+$ area of the original explanted tissue was subtracted from the terminal Tomato$^+$ area. For both E10.5 and E11.5 stages, the outgrowths of 6 sections (0-1200μm range, see Figure 5 – figure supplement 1) from each midgut segments were compiled into the dot plots. If individual explanted slices failed to stay in the collagen gel their individual data were not included in the analysis.

Wholemount immunostaining. Fixed tissues (mouse embryos, embryonic guts, postnatal gut slices, postnatal distal colon preparations) were dehydrated in a methanol series (to 100%), and bleached overnight in 3% H_2O_2 in 20% DMSO containing methanol solution. Tissues were then rehydrated in PBST (1% Tween-20 in PBST), and incubated in blocking solution (1% non-fat dried milk, 20% DMSO in PBST) for 10-60 min at room temperature followed by incubation with primary antibody in blocking solution for 2-3 days at 4°C. After extensive washes with PBST, tissues were incubated with HRP-conjugated secondary antibody (1:200, Jackson Immunoresearch) for 2-3 days at 4°C. Immunoreactive signal was then visualized by DAB detection (0.2mg/ml DAB in PBST with 0.03% H_2O_2). Stained tissues were cleared with Sca*l*eU2 (4M urea, 30% glycerol, 0.1% Triton-X 100) for imaging. Antibodies used included rabbit anti-Pax2 (1:50, Invitrogen 08-1483), rabbit anti-AP2 (1:1000, Abcam ab52222), goat anti-Sox10 (1:200, Santa Cruz sc-17342), mouse anti-HuD (1:500, Santa Cruz sc-13577), mouse anti-Tuj1 (1:1000, Biolegend MMS-435P), rabbit anti-CGRP (1:500-1000, Millipore PC205L), and rabbit anti-NOS1 (1:500, Santa Cruz sc-648). Stained tissues were cleared with Sca*l*eU2 and flat-mounted to histology slides for imaging. CGRP$^+$ afferent projections in colonic mucosa were quantified by binary threshold-level selection of the CGRP$^+$ pixel area per single villus and NOS$^+$ efferent projections were also quantified by binary threshold-level selection of NOS$^+$ pixel area in the circular muscle layer, both using Fiji-Image J software.

Wholemount immunofluorescence staining. Fixed tissues (embryonic vibratome sections, embryonic gut tissues, collagen gel cultured explants, postnatal colon vibratome sections and preparations) were permeabilized in PBST (1% Tween-20 in PBS), incubated in blocking solution (1% non-fat dried milk, 20% DMSO in PBST) for 10-60 min at room temperature followed by incubation with primary antibody in blocking solution for 2-3 days at 4°C. After extensive washing with PBST, tissues were incubated with Alexa Fluor-conjugated secondary antibody (1:500, Invitrogen) for 2-3 days at 4°C. Immunolabeled tissues were counterstained with DAPI and cleared with Sca*l*eU2 and mounted to histology slides for confocal imaging. Antibodies used were rabbit anti-Pax2 (1:50, Invitrogen 08-1483), rabbit anti-AP2 (1:1000, Abcam ab52222), goat anti-Sox10 (1:200, Santa Cruz sc-17342), mouse anti-2H3 (1:100, DSHB), chicken anti-GFP (1:3000, Abcam ab13970), goat anti-p75 (1:300, R&D systems AF1157), mouse anti-HuD (1:500, Santa Cruz sc-13577), rabbit anti-BLBP (1:500, Abcam ab32423), mouse anti-Tuj1 (1:1000, Biolegend MMS-435P), rabbit anti-CGRP (1:500-1000, Millipore PC205L), rabbit anti-NOS1 (1:500, Santa Cruz sc-648), goat anti-Ret (1:300, R&D Systems AF482), rabbit anti-phospho-Ret (Tyr1015) (1:300, ThemoFisher PA5-105930) and rabbit anti-phospho-Ret (Tyr1096) (1:300, ThemoFisher PA5-105796). Fiji Image J plugin cell counter was used for counting Tomato$^+$, CGRP$^+$, NOS$^+$, GFP$^+$, and Hu$^+$ ganglion cells in myenteric plexuses of the distal colon (defined on the basis of perfusion by the inferior mesenteric artery), and for counting Ret$^+$, phospho-Ret Tyr1015$^+$, phospho-Ret Tyr1096$^+$, and GFP$^+$ cells in E11.5 embryonic ENS wavefront cells.

Statistics. All quantified data were graphed as mean±SEM, and analyzed for significance using a two-tailed Student's t-test. Dot plots show the each individual data points and mean.

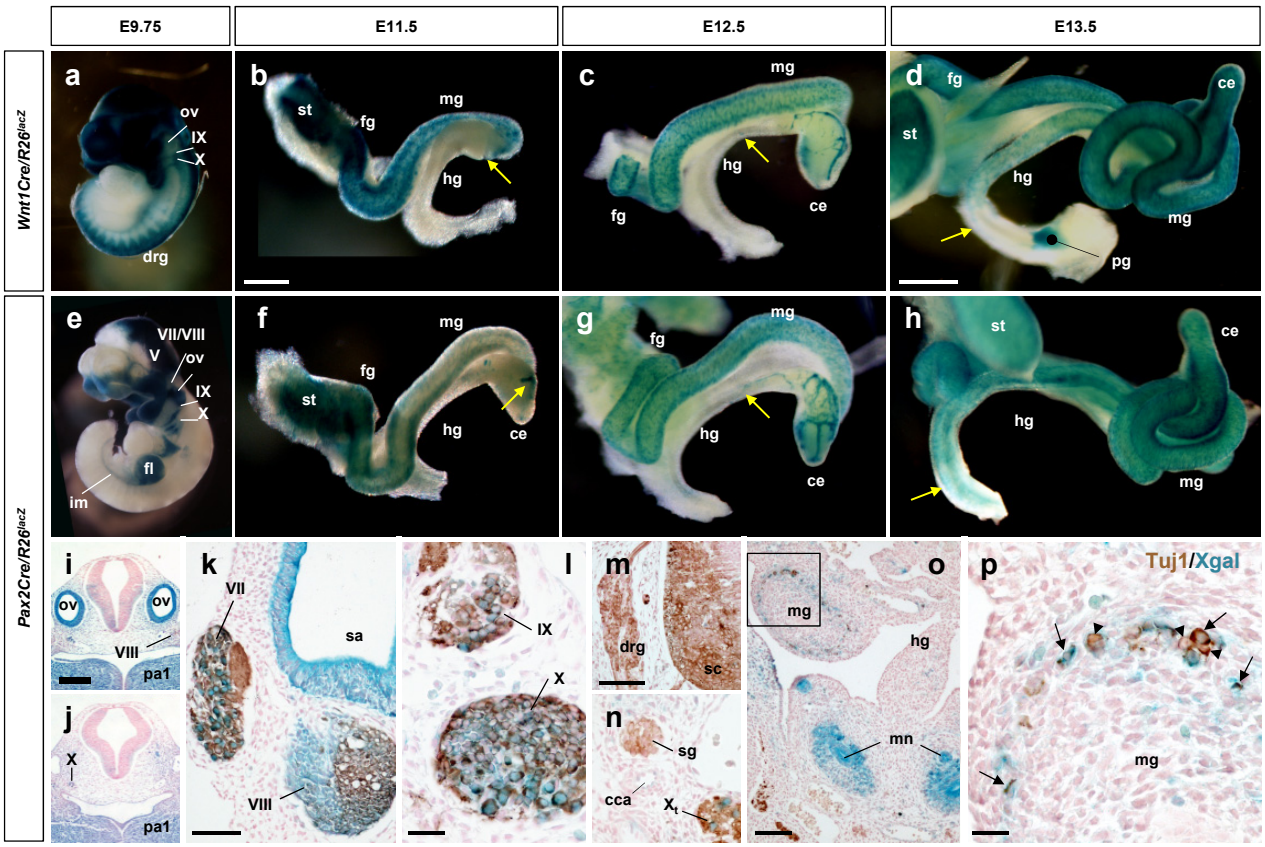

Figure 1 – figure supplement 1. Pax2Cre-derived cells contribute to the ENS. (a-h) Wnt1Cre- and Pax2Cre-lineage tracing in developing gut. Wholemount X-gal staining of *Wnt1Cre/R26^{lacZ}* (a) and *Pax2Cre/R26^{lacZ}* (e) embryos at E9.75. Wholemount X-gal stained guts isolated from *Wnt1Cre/R26^{lacZ}* (b-d) and *Pax2Cre/R26^{lacZ}* (f-h) embryos at E11.5 (b, f), E12.5 (c, g) and E13.5 (d, h). Arrows denote migrating wavefronts of Wnt1Cre-labeled (b-d) and Pax2Cre-labeled (f-h) cells on the gut walls. **(i-j)** Transverse sections of the hindbrain region of a *Pax2Cre/R26^{lacZ}* embryo at E9.5. **(k-p)** Transverse sections of E12.5 *Pax2Cre/R26^{lacZ}* embryos immunolabeled for Tuj1 (brown). Pax2Cre labels the inner ear (sa, which is otic placode-derived and non-neurogenic), and also subsets of CN V, VII, VIII, IX and X neurons (epibranchial placode-derived) (k-l), and the metanephros (o), but does not label dorsal root (m) or sympathetic ganglion (n) neurons which originate exclusively from trunk neural crest cells. Magnified view of bracketed area in o is shown in (p); arrows in (p) denote Pax2Cre-labeled Tuj1^{+} ENS neurons. Arrowheads point to Pax2Cre-unlabeled neurons. Abbreviations: cca, common carotid artery; ce, cecum; drg, dorsal root ganglion; fg, foregut; hg, hindgut; mn, metanephros; mg, midgut; ov, otic vesicle; pa, pharyngeal arch; pg, pelvic ganglion; sa, saccule; sc, spinal cord; sg, sympathetic ganglion; st, stomach. V, fifth (trigeminal) ganglion; VII, seventh (facial/geniculate) ganglion; VIII, eighth (vestibulocchlear) ganglion; IX, ninth (glossopharngeal/petrosal) ganglion; X, tenth (vagus/nodose) ganglion. Scale bars, 500µm (b-c, f-g, g-k), 1000µm (d, h), 200µm (i-j), 100µm (k, m-n, o), 25µm (l, p).

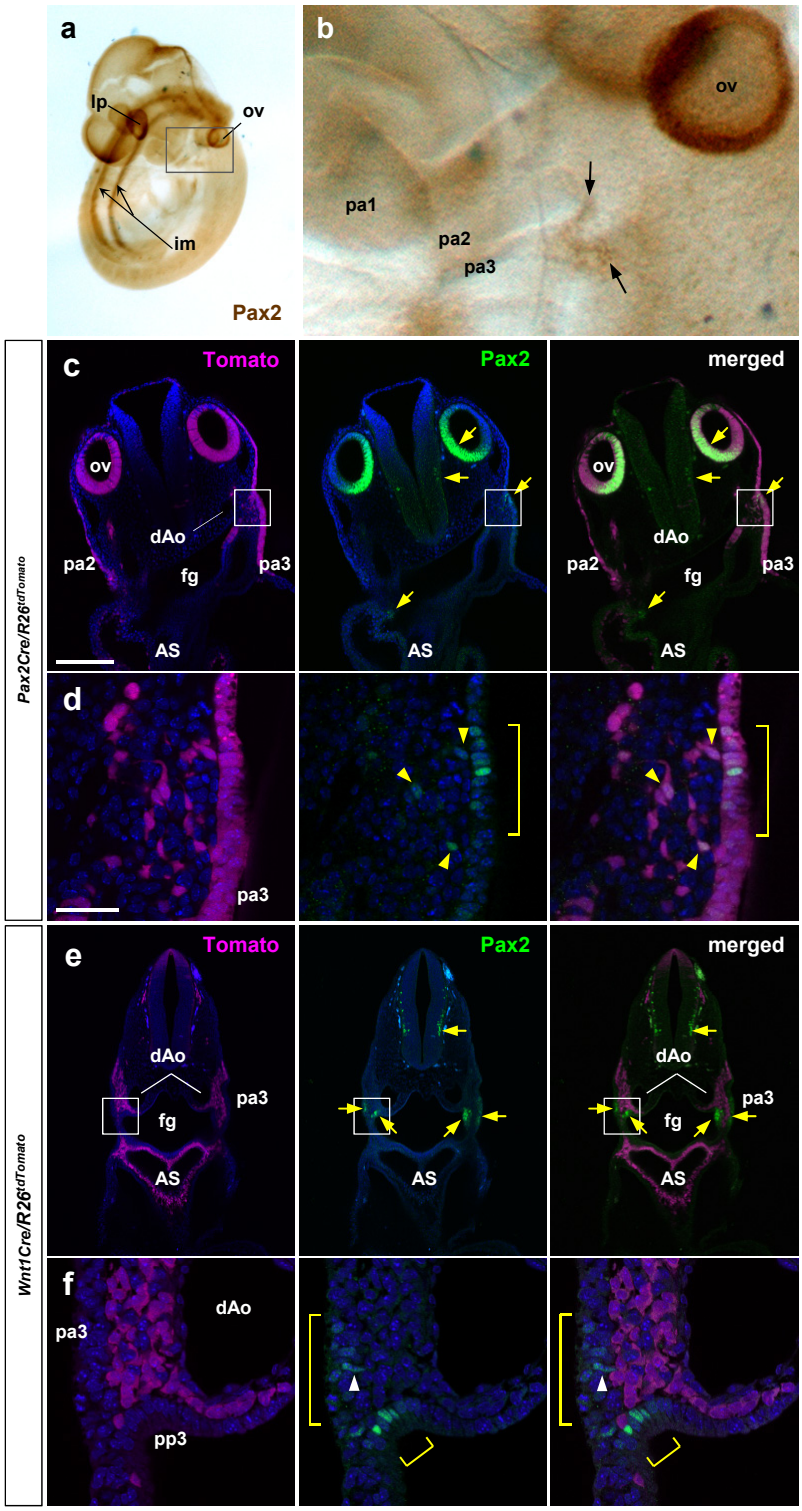

Figure 2 – figure supplement 1. Pax2Cre and Wnt1Cre label distinct early migratory cell populations. (a-b) An E9.5 wild-type embryo immunostained for Pax2 protein; (b) is a magnified view of the bracketed area including the pharyngeal arch regions in a. Arrows denote Pax2-expressing cells of the third pharyngeal cleft and pouch. **(c-f)** Vibratome sections of E9.75 *Pax2Cre/R26*^{tdTomato} (c-d) and *Wnt1Cre/R26*^{tdTomato} (e-f) embryos immunostained for Pax2. Yellow arrows denote Pax2 expression (c, e). Magnified views of bracketed area of c and e are shown in d and f. Yellow brackets denote the Pax2 expressing cells in the third pharyngeal ectoderm and endoderm (d, f). Yellow arrowheads point to Pax2-expressing Pax2Cre^{+} cells that are delaminated and migrating from the ectodermal layer (d). White arrowhead points to a Pax2-expressing Wnt1Cre-unlabeled cell that has just delaminated from the ectoderm (f). Abbreviations: AS, aortic sac; dAo, dorsal aorta; im, intermediate mesoderm; lp, lens placode; pa, pharyngeal arch; pp, pharyngeal pouch. Scale bars, 200μm (c,e), 25μm (d,f).

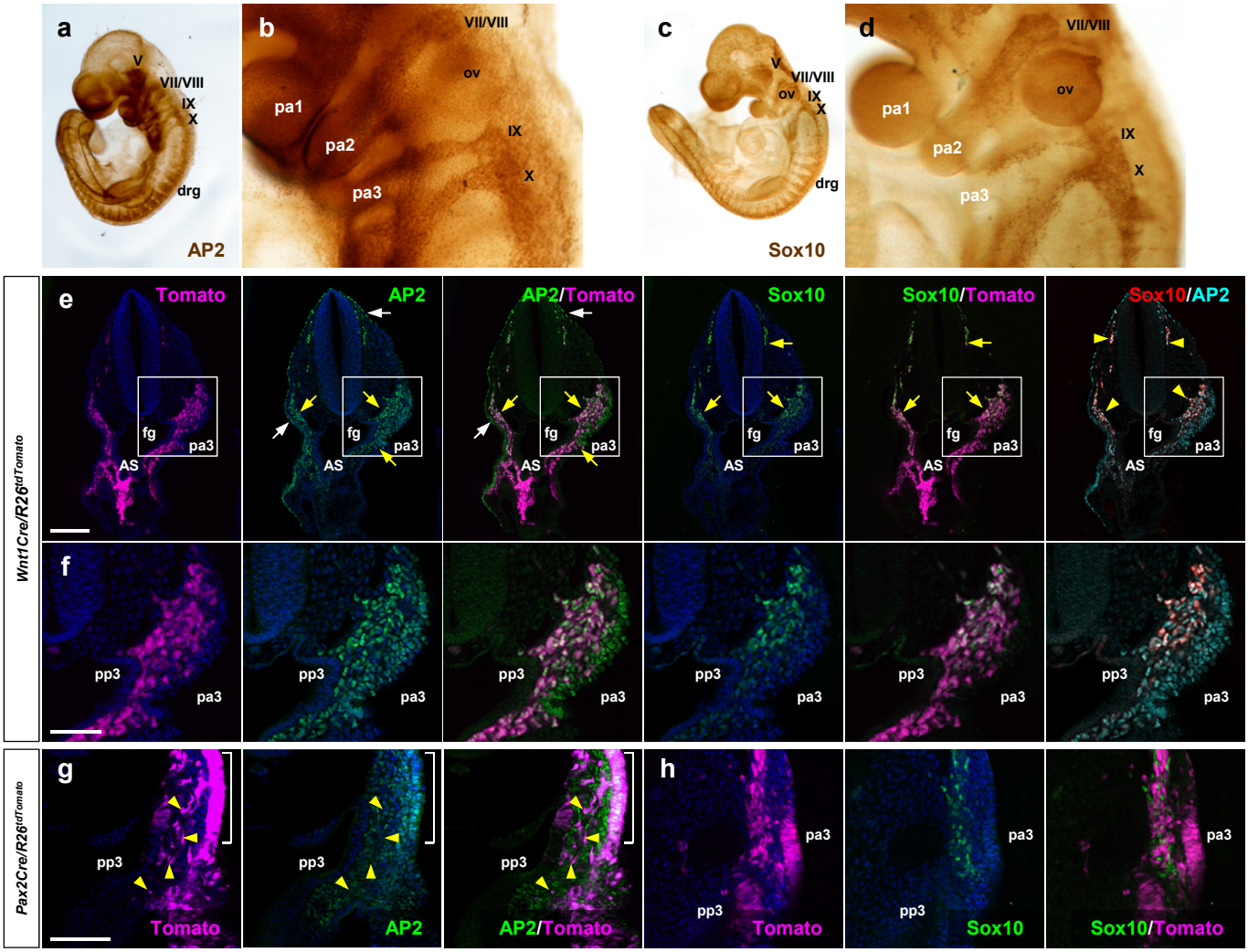

Figure 2 – figure supplement 2. Distinct lineage origin of Pax2Cre-labeled and Wnt1Cre-labeled ENS progenitor cells. (a-d) E9.5 wild-type embryos stained for AP2 (a-b) and Sox10 (c-d). Magnified views of the bracketed areas including the pharyngeal arch regions in a and c are shown in b and d, respectively. **(e-f)** Vibratome sections of E9.75 *Wnt1Cre/R26*^{tdTomato} embryo immunostained for AP2 and Sox10. White arrows denote AP2^{+} ectodermal cells. Yellow arrows indicate the Wnt1Cre-labeled neural crest cell population expressing AP2 or Sox10. Magnified views of the bracketed areas in e are shown in f. **(g-h)** Magnified views of vibratome sections of E9.75 *Pax2Cre/R26*^{tdTomato} embryo immunostained for AP2 (g) or Sox10 (h). Yellow arrowheads point to migratory Pax2Cre-derived cells with AP2-negative nuclei. Scale bars, 200μm (e), 100μm (f-h).

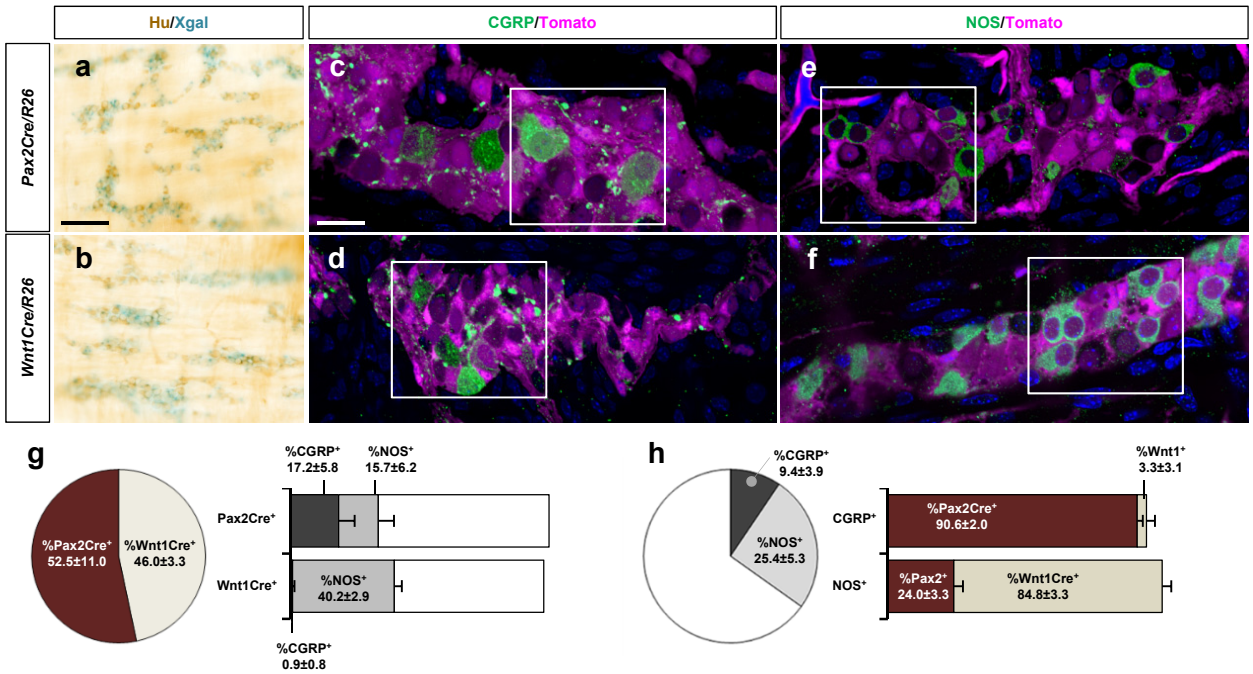

Figure 3 – figure supplement 1. Pax2Cre-derived cells preferentially give rise to CGRP⁺ myenteric neurons of the distal colon. (a-f) Wholemount preparations of P9 distal colons isolated from *Pax2Cre/R26*^{tdTomato} (a,c,e) and *Wnt1Cre/R26*^{tdTomato} (b,d,f) mice were Xgal stained and immunolabeled for Hu (a,b), or immunofluorescence labeled for CGRP (c,d) or NOS (e,f) and counterstained by DAPI. Magnified views of bracketed areas in c-f are shown in Figure 3 d-g. **(g,h)** Compiled representations of the proportion of Pax2Cre$^+$ and Wnt1Cre$^+$ neurons (g) or the proportion of CGRP$^+$ and NOS$^+$ neurons (h) among a total of 5585 myenteric neurons counted from the P9 distal colons isolated from 9 *Pax2Cre/R26*^{tdTomato} and 8 *Wnt1Cre/R26*^{tdTomato} mice (mean±s.e.m). The proportion of the CGRP$^+$ and NOS$^+$ neurons within the Pax2Cre$^+$ or the Wnt1Cre$^+$ population are presented in the bar graph of (g). The percentage of Pax2Cre$^+$ and Wnt1Cre$^+$ neurons in the CGRP$^+$ or NOS$^+$ populations are shown in the bar graph of (f). The pie charts and bar graphs do not add to 100% because these are compiled from separate and independent measurements that were compiled together graphically for ease of comparison. Error bars, mean±s.e.m. Scale bars, 100μm (a-b), 20μm (c-f).

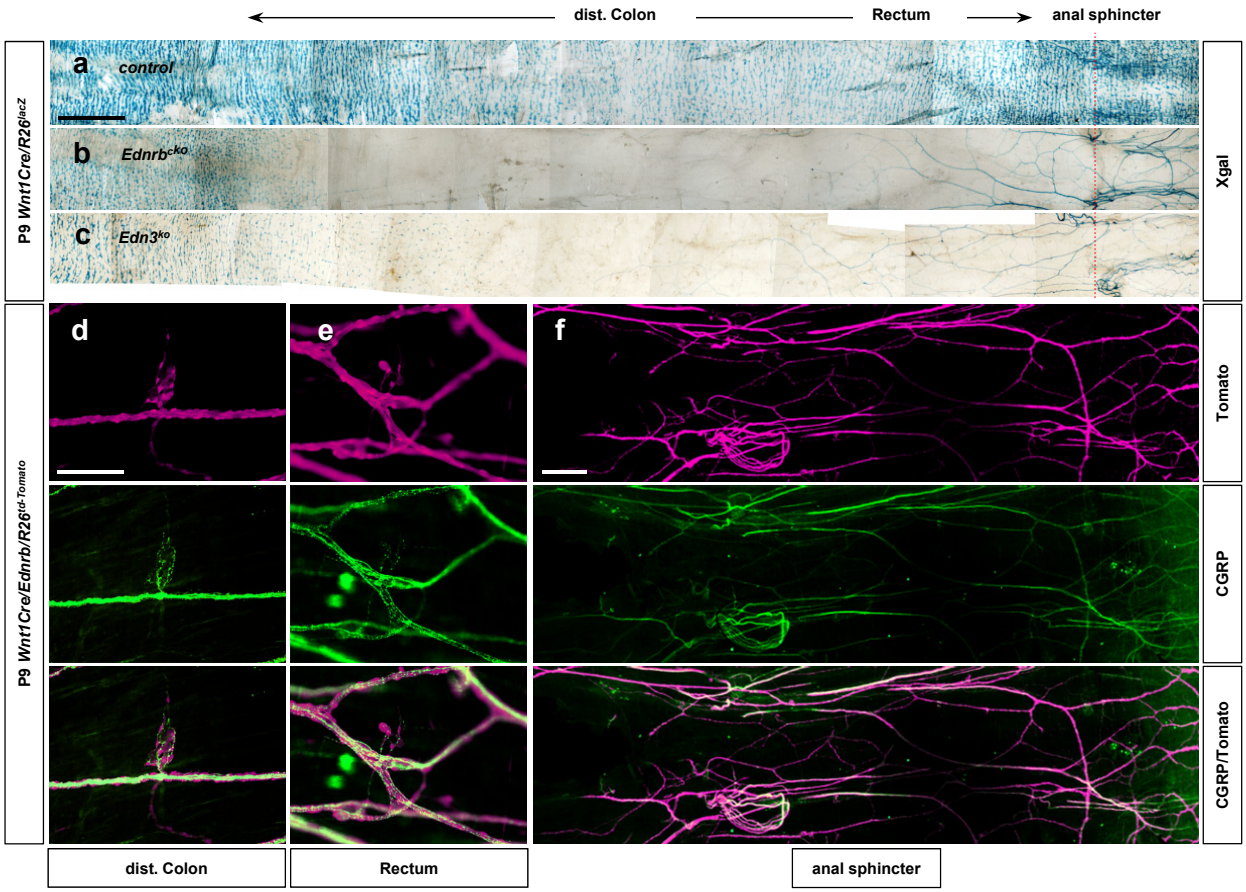

Figure 3 – figure supplement 2. Pelvic ganglion neurons and their projections express CGRP. (a-c) Distal-most end of Xgal-stained colons of the control (a), *Wnt1Cre/Ednrb* (b), and global *Edn3* (c) mutants shown in Figure 1l-n, respectively. In the absence of vagal neural crest-derived intrinsic ENS ganglia (b-c), sacral neural crest-derived pelvic ganglia and their axons become noticeable with Xgal staining. **(d-f)** Epiflurorecence microscope images of wholemount preparations of the distal colons isolated from P9 *Wnt1Cre/Ednrb/R26*$^{td\text{-}Tomato}$ mutant immunofluorescently labeled for CGRP shows sacral neural crest-derived CGPR^{+} neurons and axons in the distal colon (d), rectum (e) and anal sphincter (f) areas. Scale bars, 1000μm (a-c), 100 μm (d-e), 500 μm (f).

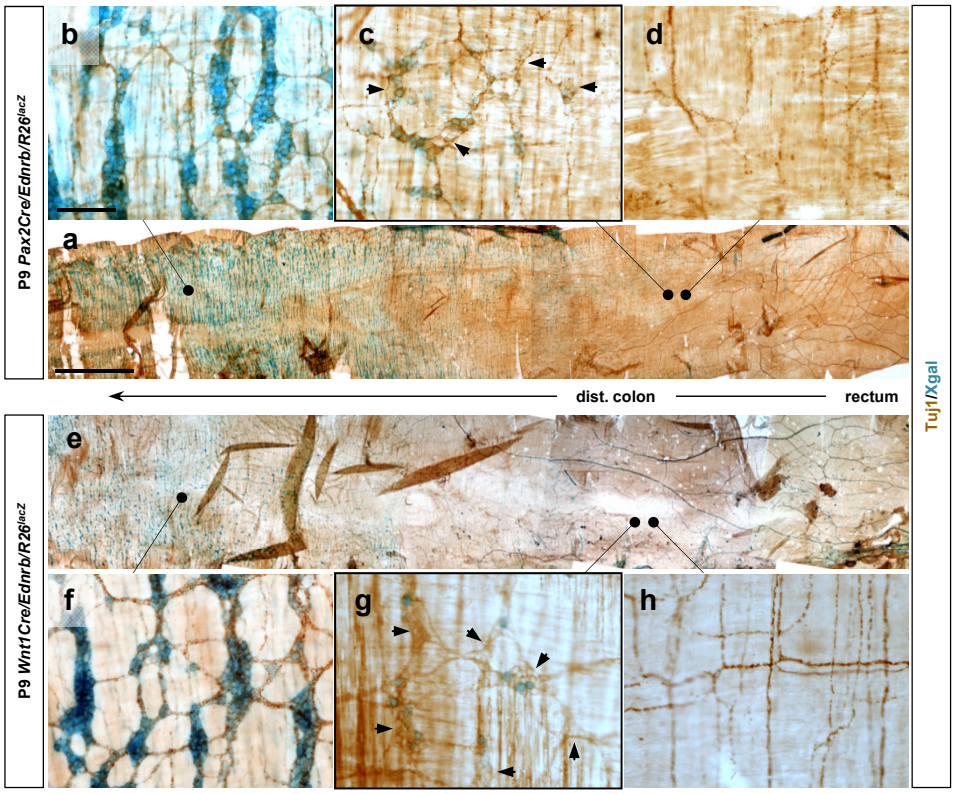

Figure 3 – figure supplement 3. Transition areas in lineage-specific *Ednrb* mutant distal colon also contain lineage-unlabeled neurons. (a,e) Wholemount preparations of P9 distal colons isolated from *Pax2Cre/Ednrb* (a) and *Wnt1Cre/Ednrb* (e) stained with Xgal and for Tuj1 to visualize lineage-labeled and lineage-unlabeled neurons and their axons. **(b-c,f-h)** Magnified views showing myenteric plexus morphology in the areas that are normally colonized (b,f), at the location of terminal migration (c,g), and at a location immediately beyond the point of terminal migration (d,h). Residual Tuj1 signal in axons in d and h are extrinsic nerves. Histological analysis for CGRP and NOS in Figure 3h-o was performed with segments equivalent to the location of panels c and g. Arrows in c and g point to lineage-unlabeled cells of myenteric ganglia. Scale bars, 1000μm (a, e), 100μm (b-d, f-h).

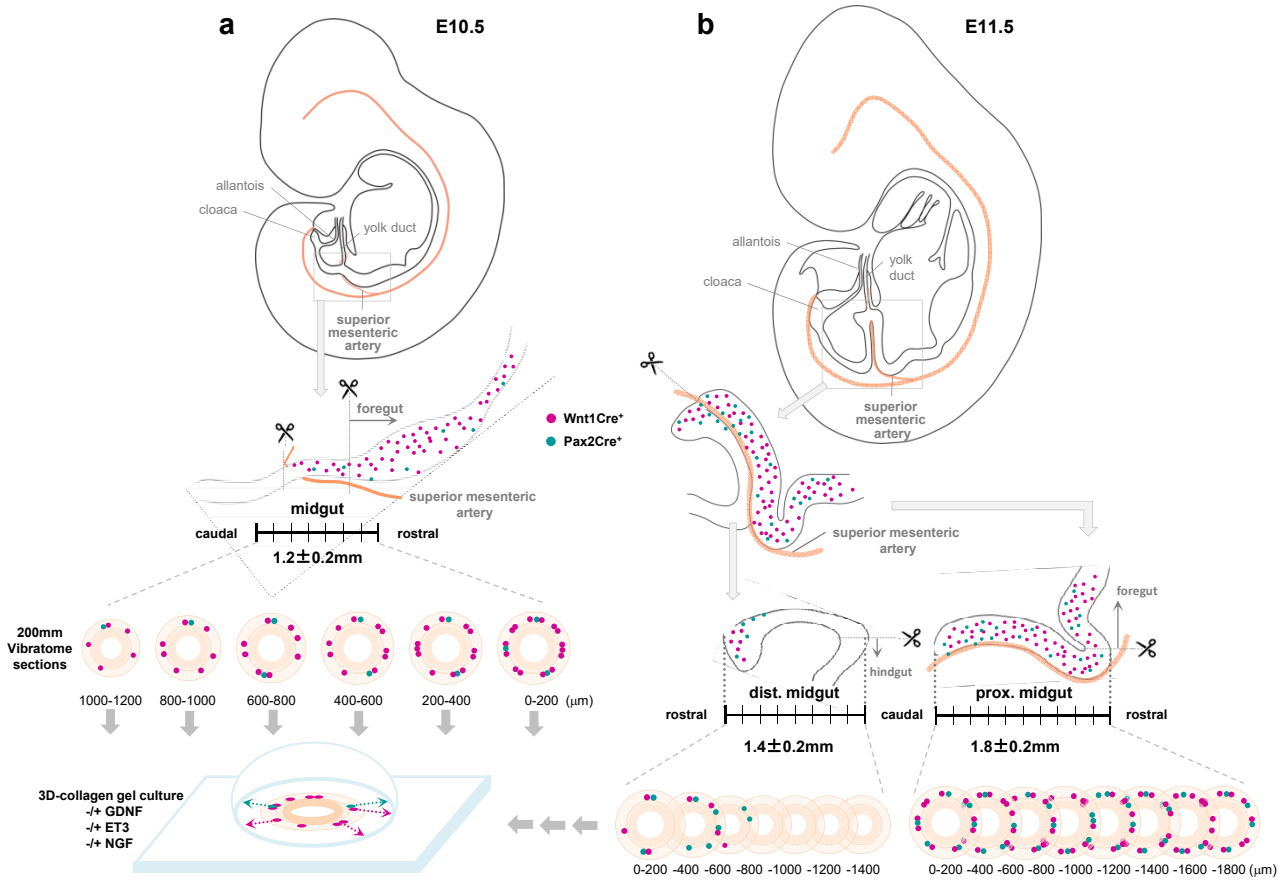

Figure 5 – figure supplement 1. Schematic illustrations of rostrocaudal orientation of gut slice explant culture. (a) E10.5 midgut slice preparation. The midgut segment was isolated based on the origin of the superior mesenteric artery from the dorsal aorta (cranial end) to where it meets the yolk (vitelline) duct. 200μm vibratome sections were prepared in a rostral to caudal direction and individually cultured in collagen gel in the absence or presence of GDNF, EDN3 or NGF. **(b)** E11.5 midgut slice preparation. First, the whole gut tissue (from stomach through cloaca) was excised from E11.5 embryo, and then the midgut loop was isolated. The proximal midgut segment was dissected by separating the midgut loop along the superior mesenteric artery and then by removing the foregut portion at the cranial end of the superior mesenteric artery. The superior mesenteric artery was kept with the proximal midgut segment for the rest of the procedure. The hindgut was then removed from the distal midgut segment based on the position of the inferior mesenteric artery. For both proximal and distal midgut segments, 200μm vibratome sections were prepared in ventral to dorsal direction and individually cultured in collagen gel in the absence or presence of GDNF, EDN3 or NGF. E10.5 midgut tissues that were larger or smaller than 1200±200μm, and E11.5 gut tissues with proximal midgut segments larger or smaller than 1800±200μm, were considered as over- or underdeveloped and excluded from further analysis. See Supplemental Methods section for details.

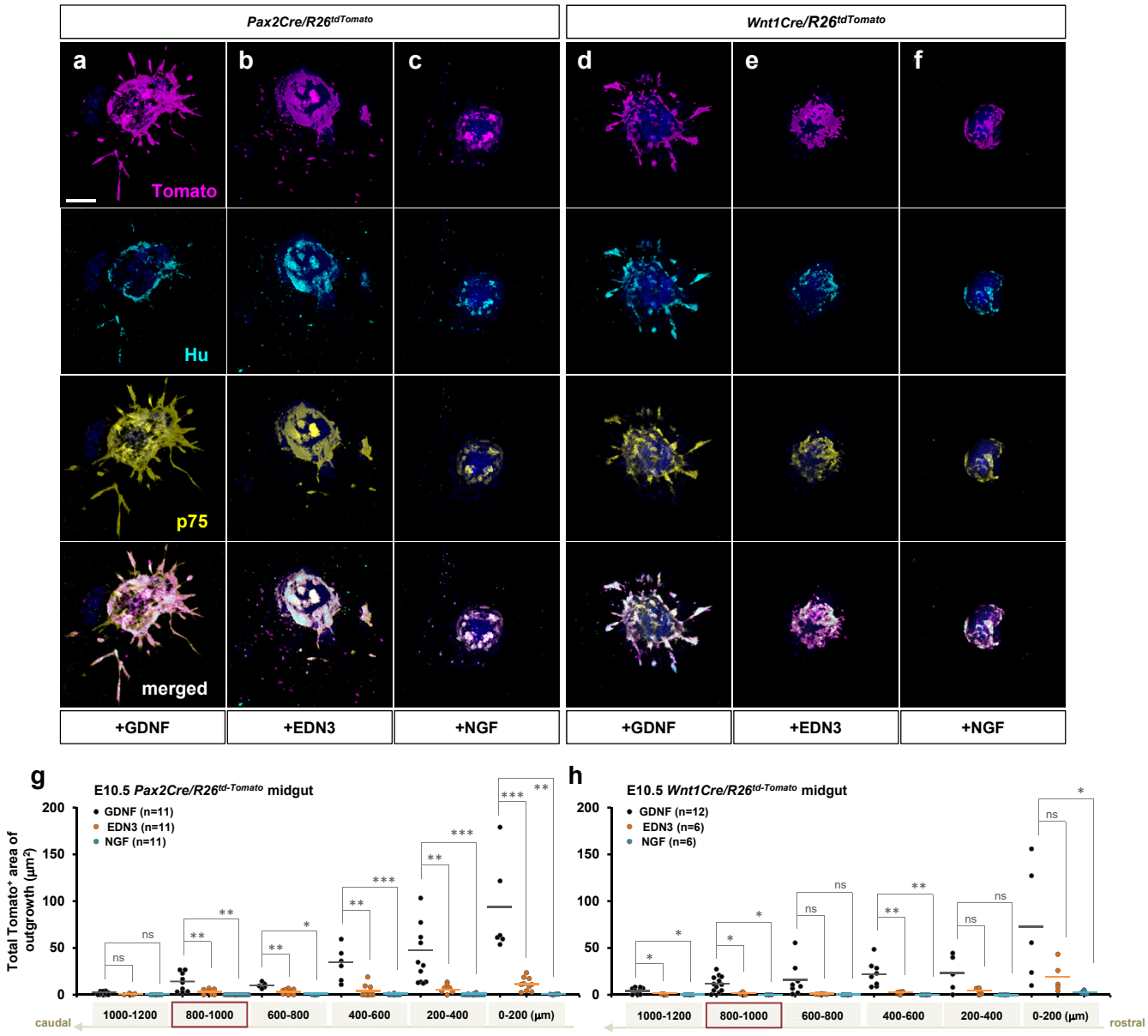

Supplemental Figure S8. EDN3 exhibited marginal effects on E10.5 enteric progenitor outgrowth in vitro. (a-f) Confocal z-stack images of 200µm midgut sections isolated from E10.5 *Pax2Cre/R26*$^{td\text{-}Tomato}$ (a-c) and *Wnt1Cre/R26*$^{td\text{-}Tomato}$ embryos cultured for 3 days in the presence of GDNF (a), EDN3 (b) or NGF (c) and stained for neuronal Hu (cyan) and ENS progenitor marker p75 (yellow). Scale bar, 250µm. **(g,h)** Compiled representations of the total area of outgrowth (Tomato^{+} area around the explanted gut tube) from *Pax2Cre/R26*$^{td\text{-}Tomato}$ and *Wnt1Cre/R26*$^{td\text{-}Tomato}$ midgut slice explants in the presence of GDNF (black), EDN3 (orange), or NGF (blue). The data from GDNF treated groups here are shown as the controls in Figure 5. See Figure 5 – figure supplement 1a for rostrocaudal orientation of these midgut slice preparations. Each dot represents one gut slice isolated from the indicated axial level; lost sections were not included as data points. The images shown in a-f represent sections that are 800-1000µm caudal to the foregut-midgut junction (red boxes in g and h). P-values: *$p<0.05$, **$p<0.01$, ***$p<0.001$, ns=not significant.

Poltavski_Figure 6 – figure supplement 1

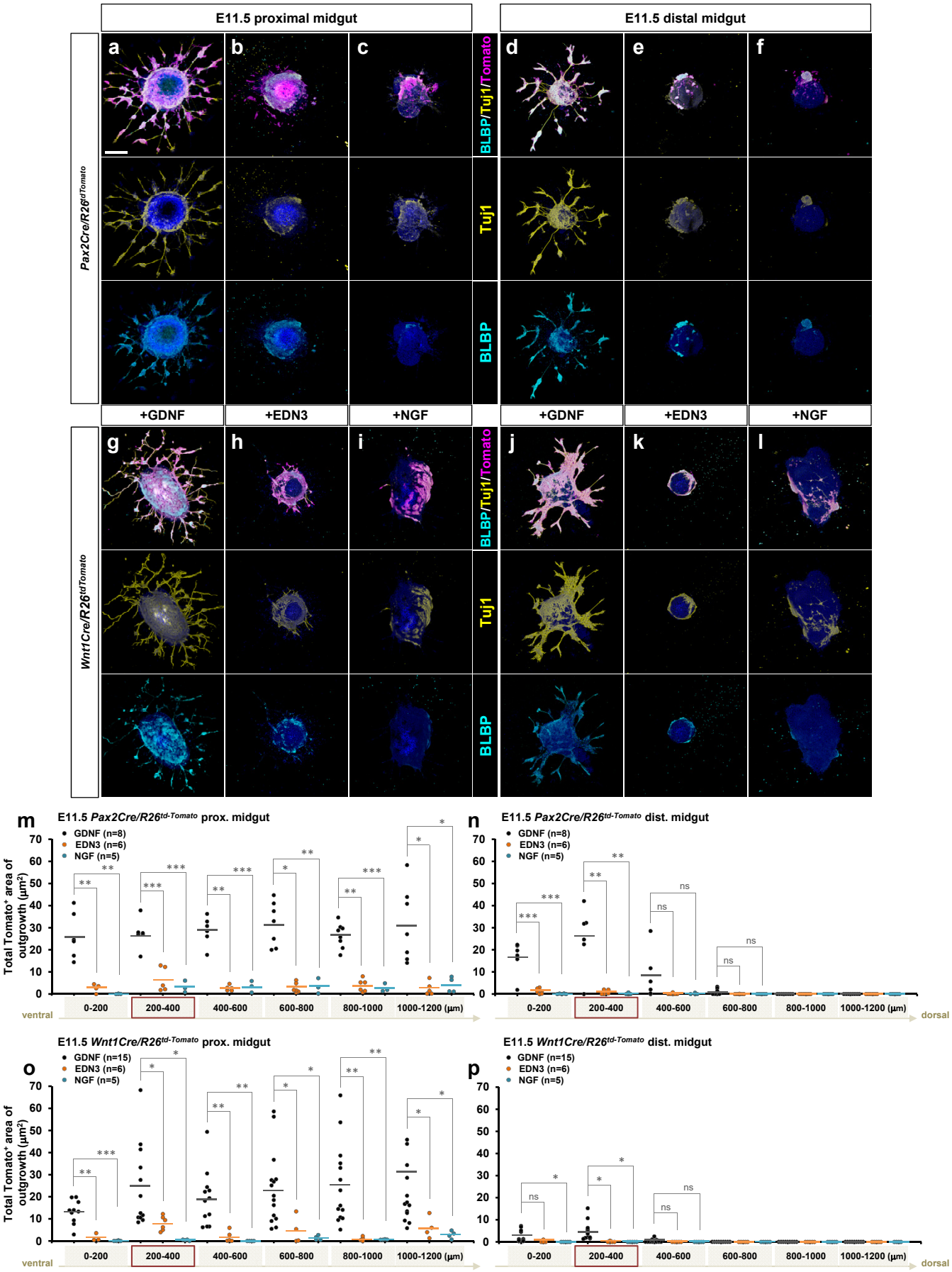

Figure 6 – figure supplement 1. EDN3 exhibits minimal effect on E11.5 enteric progenitor outgrowth *in vitro*. (a-h) Confocal z-stack images of 200μm proximal (a-c, g-i) and distal midgut (d-f, j-l) sections isolated from E11.5 *Pax2Cre/R26*$^{td\text{-}Tomato}$ (a-f), *Wnt1Cre/R26*^{tdTomato} (g-l) embryos cultured for 3 days in the presence of GDNF (a, d, g, j), EDN3 (b, e, h, k) or NGF (c, f, I, l), and then stained for neuronal Tuj1 (yellow) and glial BLBP (cyan). Scale bars, 250μm (a-f). **(m-p)** Compiled representations of the total area of outgrowth in the presence of GDNF, EDN3, vs. NGF from proximal (m, o) and distal (n, p) midgut slice explants prepared from E11.5 *Pax2Cre/R26*$^{td\text{-}Tomato}$ (m-n) and *Wnt1Cre/R26*^{tdTomato} (o-p) embryos. The data from GDNF treated groups here are shown as the controls in Figure 6. See Figure 5 – figure supplement 1b for rostrocaudal orientation of the midgut slice preparation. The proximal midgut images shown in a-c and g-i represent sections that are 200-400 μm rostral to the apex of the midgut loop, the distal midgut images shown in d-f and j-l represent sections that are 200-400 μm caudal to the apex of the midgut loop (red boxes in m-p). P-values: *$p<0.05$, **$p<0.01$, ***$p<0.001$, ns=not significant.

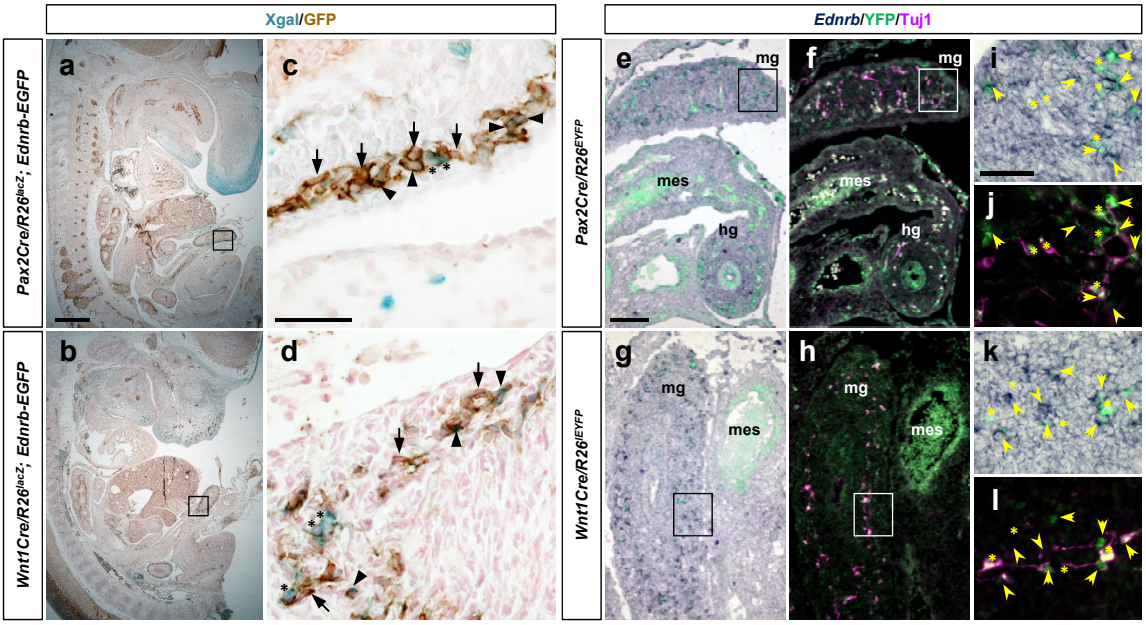

Figure 7 – figure supplement 1. Ednrb is expressed in subsets of Pax2Cre- and Wnt1Cre-derived enteric progenitor cells. (a-d) Histological sections of Xgal stained E12.5 *Pax2Cre/R26^{lacZ}; Ednrb-EGFP* (a) and *Wnt1Cre/R26^{lacZ}; Ednrb-EGFP* embryos immunolabeled for GFP. Magnified views of braketed areas in a and b are shown in c and d, respectively. Arrowheads point to Xgal^{+}/GFP^{+} cells, asterisks denote Xgal^{+}/GFP^{-} cells, and arrows point to Xgal^{-}/GFP^{+} cells in c and d. **(e-h)** Cryosections of E12.5 *Pax2Cre/R26^{EYFP}* (e-f) and *Wnt1Cre/R26^{EYFP}* (g-h) embryos at the midgut-hindgut area labeled by *in situ* hybridization for *Ednrb* gene (purple), and immunolabeled for GFP (green) and Tuj1 (magenta). Brightfield images of *Ednrb* transcripts overlaid with lineage marker YFP are shown in e and g, and their fluorescence images of YFP and Tuj1 reactive signals are shown in f and h. Magnified views of bracketed areas in e,g are shown in I,k, and in f,h in j,l. mes, mesentery. Arrows denote YFP^{+}/*Ednrb*$^{+}$ cells, asterisks indicate YFP^{+}/*Ednrb*$^{-}$ cells, and arrowheads point to YFP^{-}/*Ednrb*$^{+}$ ENS cells. Scale bars, 250μm (a-b), 50μm (c-d, i-l), 100μm (e-h).